Full Title

Pharyngeal motor cortex grey matter abnormalities and retinal photoreceptor layer dysfunction in macaques exposed to Zika virus in utero

Short Title

Brain abnormalities in infant macaques exposed to Zika virus in utero

Authors

Michelle R. Koenig[1,3], Elaina Razo[2], Ann Mitzey[3], Matthew R. Semler[1], Laurel M. Stewart[1], Meghan E. Breitbach[1], Christina M. Newman[1], Dawn M. Dudley[1], Andrea M. Weiler[4], Sierra Rybarczyk[4], Kathryn M. Bach[9], Mariel S. Mohns[1], Heather A. Simmons[4], Andres Mejia[4], Maria Dennis[15], Leandro B. C. Teixeira[5], Michele L. Schotzko[4], T. Michael Nork[6], Carol A. Rasmussen[6], Alex Katz[6], Jiancheng Hou[7], Amy Hartman[8], James Ver Hoeve[6], Charlene Kim[6], Mary L. Schneider[9], Karla Ausderau[9], Sarah Kohn[7], Anna S. Jaeger[10], Matthew T. Aliota[10], M. Shahriar Salamat[1], Jennifer M. Hayes[4], Nancy Schultz-Darken[4], Jens Eickhoff[16], Kathleen M. Antony[11], Kevin Noguchi[12], Xiankun Zeng[13], Sallie Permar[15], Chrysanthy Ikonomidou[14], Vivek Prabhakaran[7], Saverio Capuano III[4], Thomas C. Friedrich[4,5], Thaddeus G. Golos[3,4,11], David H. O'Connor[1,4], Emma L. Mohr[2]

Affiliations

1 Department of Pathology and Laboratory Medicine, UW-Madison, Madison, Wisconsin, USA

2 Department of Pediatrics, UW-Madison, Madison, Wisconsin, USA

3 Department of Comparative Biosciences, UW-Madison, Madison, Wisconsin, USA

4 Wisconsin National Primate Research Center, UW-Madison, Madison, Wisconsin, USA

5 Department of Pathobiological Sciences, UW-Madison, Madison, Wisconsin, USA

6 Department of Ophthalmology and Visual Sciences, UW-Madison, Madison, Wisconsin, USA

7 Department of Radiology, UW-Madison, Madison, Wisconsin, USA

8 Department of Communication Sciences and Disorders, UW-Madison, Madison, Wisconsin, USA

9 Department of Kinesiology, UW-Madison, Madison, Wisconsin, USA

10 Department of Veterinary and Biomedical Sciences, University of Minnesota, Minneapolis, Minnesota, USA

11 Department of Obstetrics and Gynecology, UW-Madison, Madison, Wisconsin, USA

12 Department of Psychiatry, Washington University School of Medicine, Saint Louis, Missouri, USA

13 United States Army Medical Research Institute of Infectious Diseases, Fort Detrick, Frederick Maryland, USA

14 Department of Neurology, UW-Madison, Madison, Wisconsin, USA

15 Department of Pediatrics, Duke University, Durham, North Carolina, USA

16 Biostatistics and Medical Informatics, UW-Madison, Madison, Wisconsin, USA

Abstract

One third of infants who have prenatal Zika virus (ZIKV) exposure and lack significant defects consistent with congenital Zika syndrome (CZS) manifest neurodevelopmental deficits in their second year of life. We hypothesized that prenatal ZIKV exposure would lead to brain abnormalities and neurodevelopmental delays in infant macaques, as measured by quantitative hearing, neurodevelopmental, ocular and brain imaging studies.

We inoculated 5 pregnant rhesus macaques with ZIKV during the first trimester, monitored pregnancies with serial ultrasounds, determined plasma viral RNA (vRNA) loads, and evaluated the infants for birth defects and neurodevelopmental deficits during their first week of life. ZIKV-exposed and control infants (n=16) were evaluated with neurobehavioral assessments, ophthalmic examinations, optical coherence tomography, electroretinography with visual evoked

potentials, hearing examinations, magnetic resonance imaging (MRI) of the brain, gross post mortem examination, and histopathological and vRNA analyses of approximately 40 tissues and fluids. All 5 dams had ZIKV vRNA in plasma and seroconverted following ZIKV inoculation. One pregnancy resulted in a stillbirth. The ZIKV-exposed infants had decreased cumulative feeding volumes and weight gains compared with control infants, and also had grey matter abnormalities in the pharyngeal motor cortex identified by quantitative voxel-based morphometric comparisons. Quantitative ocular studies identified differences between ZIKV-exposed and control infants in retinal layer thicknesses and electroretinograms that were not identified in qualitative ophthalmic evaluations. Despite these findings of neuropathology, no ZIKV vRNA or IgM was detected in the infants. This suggests that ZIKV exposure without measurable vertical transmission can affect brain development in utero and that subtle neurodevelopmental delays may be detected with quantitative analyses in early infancy. Quantitative brain analyses, such as these, may predict neurodevelopmental delays that manifest later in childhood and allow early intervention and targeted therapies to improve functional outcomes of ZIKV exposed children.

Author Summary

Human infants with born to women with Zika virus infection during pregnancy are at risk for neurodevelopmental deficits later in childhood. We hypothesized that we could identify brain abnormalities associated with neurodevelopmental deficits in infant macaques exposed to Zika virus during pregnancy. We identified brain and retinal abnormalities in Zika virus-exposed infant macaques during their first week of life, which may be related to their findings of decreased feeding and slower weight gain. None of the infants had direct evidence of Zika virus infection in their tissues, body fluids or by detection of IgM antibodies. This suggests that Zika virus exposure during pregnancy can affect brain development in utero and that quantitative

brain imaging analyses may predict neurodevelopmental delays. Early identification of Zika virus-exposed children at risk of neurodevelopmental deficits would promote targeted therapies in this population and improve the functional outcome of all Zika virus exposed children.

Introduction

Zika virus (ZIKV) infection during pregnancy can result in birth defects and neurodevelopmental abnormalities in infants which include: brain abnormalities leading to neurodevelopmental deficits, ocular abnormalities that impair vision, auditory abnormalities and dysfunction, and joint and limb contractures (1). Approximately 7-13% of infants who are exposed to maternal ZIKV infection have neurologic and ocular abnormalities (2), with more significant impacts when infants are exposed earlier in pregnancy (2-5). Birth defects associated with congenital ZIKV syndrome (CZS) can be diagnosed with a combination of physical examination, ocular and acoustic studies, and diagnostic imaging in the early neonatal period (6). Some deficits are only diagnosed when infants fail to meet developmental milestones (7). Children who were born during the 2015-2016 ZIKV epidemic in the western hemisphere are now reaching the age where neurodevelopmental deficits that could not be identified at birth are being described in longitudinal studies (7-10). Not surprisingly, longitudinal studies show that children with CZS have severe gross motor, fine motor and problem-solving skills (7, 8). What was not expected is the finding that one third of infants who were asymptomatic at birth, meaning that they did not have any findings consistent with CZS, developed mild to moderate neurological abnormalities during their second year of life (9, 10). These are the earliest reports of long-term neurodevelopmental outcomes of children who were asymptomatic at birth and may just be the beginning of additional human cohort studies describing neurodevelopmental deficits in prenatally ZIKV-exposed infants and children.

Longitudinal observations of infants and children affected by prenatal exposure to ZIKV are necessary to fully define the spectrum of disorders and identify adjunctive therapies necessary to improve functional outcomes. However, such longitudinal human cohort studies are not designed to define disease pathogenesis or predict functional outcomes because the infants included differ in ZIKV fetal exposure times during gestation, ZIKV strains, and socioeconomic backgrounds. The heterogeneous nature of ZIKV human observational trials is one reason why translational models of ZIKV infection during pregnancy have been developed. These translational models, particularly the macaque model, are used to study ZIKV pathogenesis to better understand how maternal ZIKV infection leads to birth defects and neurodevelopmental deficits, with the end goal of identifying targets for intervention and therapy (11-13).

Studies in macaque models to assess the effect of maternal ZIKV infection on pregnancy and fetuses to-date have utilized pregnancy-related or birth outcome-related endpoints (ie fetal demise or microcephaly) to define disease pathogenesis and the spectrum of disease. No macaque models of congenital ZIKV infection have defined long-term outcomes of the macaque infants in the postnatal period or performed evaluations on the infants that mirror the clinical evaluation that human infants receive when born to a mother with confirmed ZIKV infection during pregnancy (6). Infant macaques who are infected with ZIKV as neonates had altered emotional reactivity to acute stress, likely due to altered functional connectivity between specific brain regions (14), but ZIKV infection in the neonatal period cannot necessarily be applied to fetal ZIKV infection or exposure. However, this small study of infant ZIKV infection indicated that macaque infants can be used successfully to study neurodevelopment in the postnatal period.

Here, we describe the development of the first comprehensive evaluation for birth defects and neurodevelopmental abnormalities after birth in a macaque model of maternal ZIKV infection. We modeled our macaque infant assessments on the recommended evaluation panel for

human infants born to women with laboratory evidence of confirmed or possible ZIKV infection (6). We exceeded recommended human infant testing by defining how fine anatomic differences lead to changes in functional outcomes by quantitatively evaluating brain structure and visual function. Here we describe the development of the first comprehensive postnatal assessment of infant macaques with prenatal ZIKV exposure in first trimester and define changes in the brain and retina that are associated with changes in neurodevelopmental outcomes, including feeding and visual function.

Results

ZIKV inoculation during pregnancy

Five dams were inoculated with ZIKV in the first trimester (41-50 gd) (Table 1). None of the dams had fever, rash, or inappetence following inoculation. One dam (664184) had a stillbirth at gestational day 133 and the fetus was found partially delivered; the remaining infants were delivered by Cesarean delivery at 154-155 gd (term = 165 gd) (Fig 1A) to ensure collection of maternal-fetal interface (MFI) tissues. Maternal plasma viral loads peaked 3-5 days post inoculation in all animals. Four of the five animals had detectable viremia for at least 28 days (664184, 484880, 795784, 918724). One animal (730267) resolved viremia within 6 days (Fig 1B). ZIKV-specific neutralizing antibodies were detected by 28 dpi and persisted until the last time point measured at necropsy (Fig 1C). Only the 28 dpi and necropsy timepoints demonstrated measurable levels of ZIKV-specific IgG in a whole virion ELISA (Fig 1D, with dose response curves demonstrated in S1 figure). Dams 664184 and 484880 had lower neutralizing antibody titers at necropsy than at 28 dpi, and 484880 also had a lower ZIKV-specific IgG response at necropsy compared with 28 dpi.

Table 1. Characteristics of the dams inoculated with ZIKV.

	Dam ID				
	664184	484880	795784	918724	730267
Maternal age at conception (years)	4	11	16	14	13
Number of prior pregnancies	0	5	4	7	6
Gestational age at ZIKV inoculation (days)	46	43	41	50	44

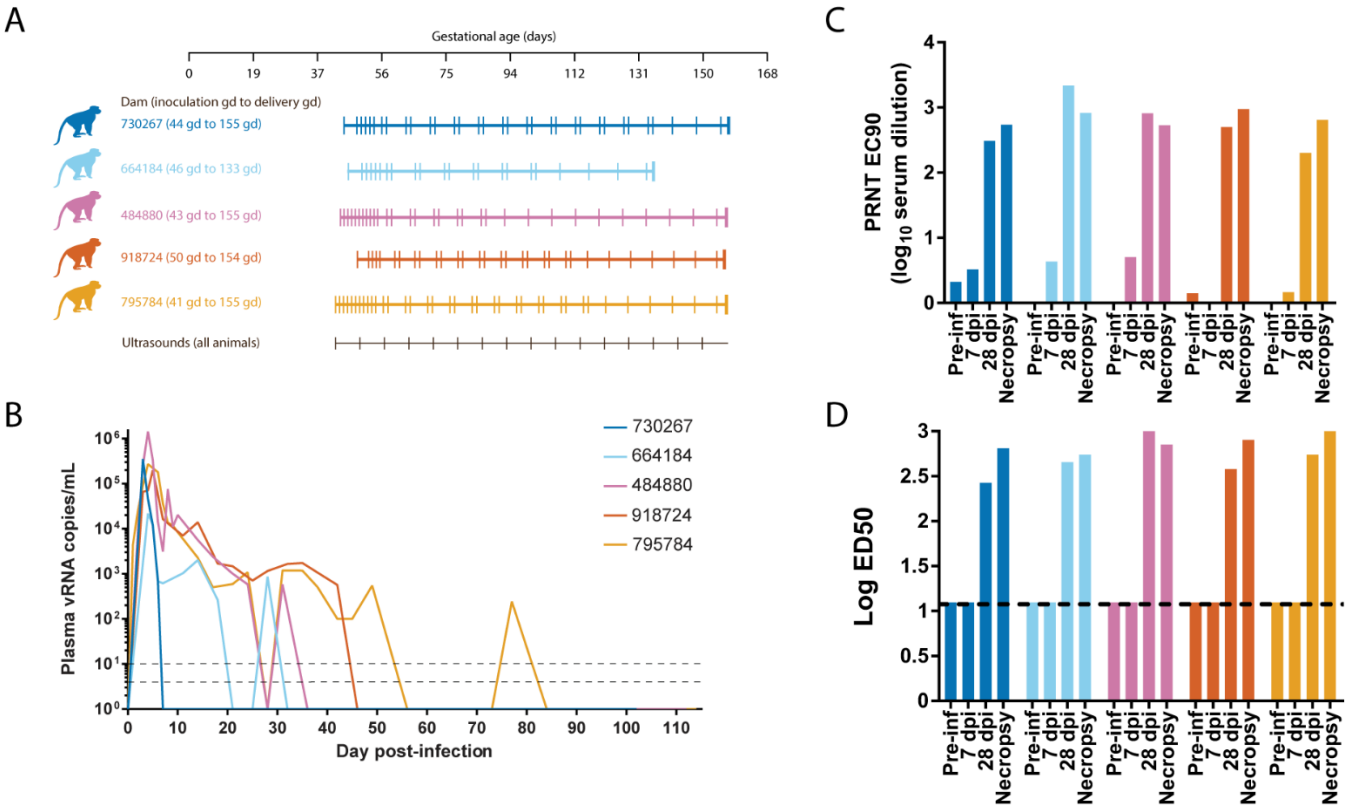

Figure 1. Pregnancy experimental design, maternal plasma vRNA loads and maternal antibody responses.

Pregnancy course and fetal ultrasonography

Given the association of microcephaly and low birthweight with congenital ZIKV infection (1), we monitored fetal growth closely with serial ultrasounds. In humans, fetal microcephaly is typically defined as more than 3 SD below the mean head circumference and a fetal head circumference at 2 SD below the mean warrants a more detailed analysis of intracranial anatomy (15). In our ZIKV-exposed pregnancies, none of the fetuses had a head circumference or biparietal diameter more than 2 SD below the mean in the ultrasound immediately prior to delivery (Fig 2). Some of the fetuses (3 of 5) had a head circumference more than 2 SD below the mean approximately 2 weeks before delivery and all of these increased to less than 2 SD below the mean in the ultrasound immediately prior to delivery. This indicates that although there was variability in head circumference compared with the mean during gestation, none would classify as microcephalic (greater than 3 SD below the mean) immediately before birth. Biparietal diameter measurements appeared to have less variability than the head circumference measurements, with no biparietal diameter measurements greater than 2 SD below the mean in the last 60 days of gestation (Fig 2). None of the fetuses had a femur length or abdominal circumference that was greater than 2 SD below the mean just prior to delivery (S2 figure).

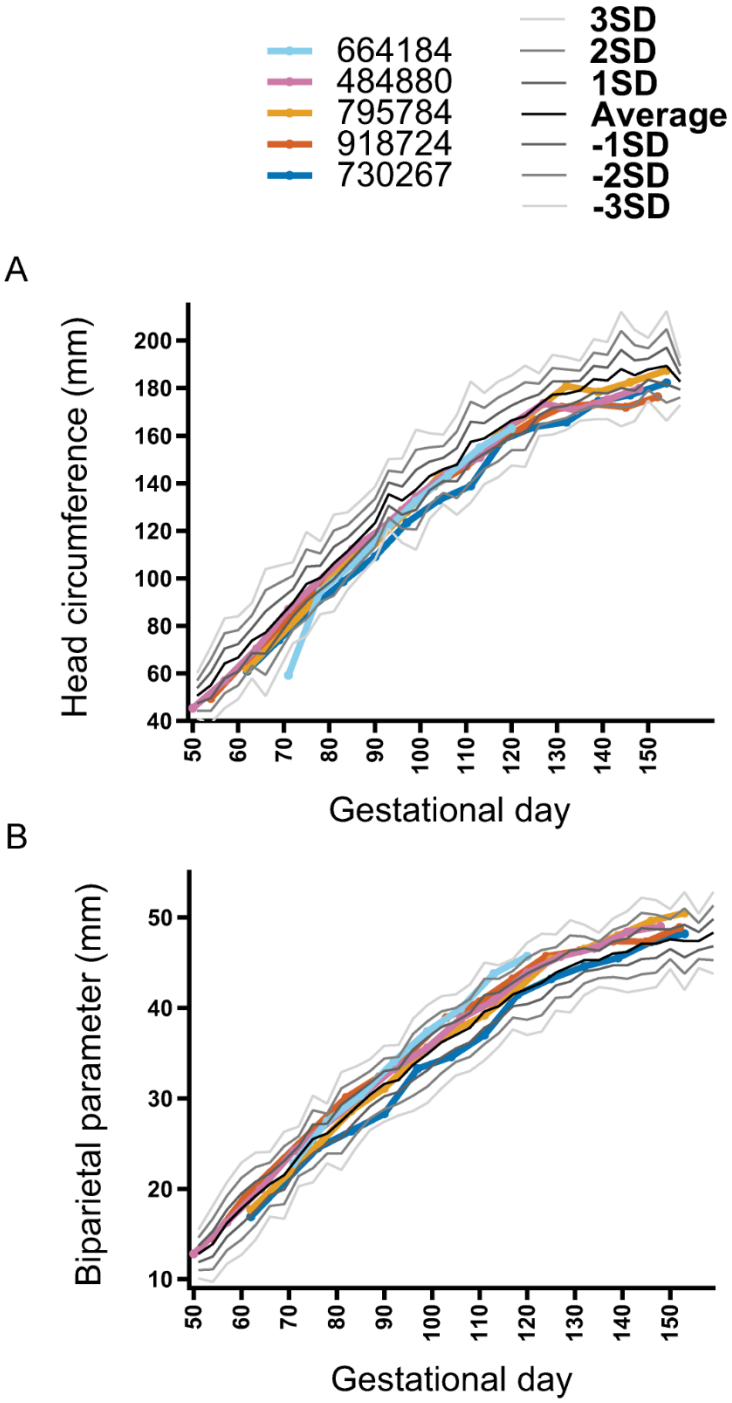

Figure 2. Fetal head growth during pregnancy.

Fetal heart rates were measured biweekly as an indirect measurement of fetal well-being. One of the five ZIKV-infected dams (664184) had a decreased fetal heart rate (bradycardia) from gd85 until stillbirth at gd133 when the fetus (416597) was found partially delivered (S2 figure). The remaining four fetuses had consistent heart rates above 150 beats per minute with no life-threatening events in utero.

Morphologic abnormalities were identified in the weekly fetal ultrasounds. Two fetuses had pericardial effusions (from dams 918724 and 795784) that appeared intermittently in ultrasounds. The pericardial effusion appeared physiologic (within normal limits) in the fetus of 918724 and was no longer visualized on ultrasound due to fetal position just prior to delivery in the fetus of 795784. The fetus from dam 730267 had a hyperechoic area within the liver noted at multiple time points (S3 figure). The pericardial effusions were not thought to be clinically significant because they did not persist throughout the pregnancy. Hepatic hyperechoic regions have been associated with other congenital infections, but may also be unrelated.

Maternal-fetal interface vRNA tissue distribution and histopathology

Histologic evaluation of maternal-fetal interface (MFI) tissues (placenta, decidua, and uterine placental bed) of the 5 ZIKV-inoculated dams and a mock (PBS)-inoculated dam (dam 020101) revealed some degree of maternal vascular malperfusion in all pregnancies including the control. There was neutrophilic deciduitis (4/5 ZIKV-infected pregnancies, not in the control) and chronic plasmacytic deciduitis (3/5 ZIKV-infected pregnancies and 1 control pregnancy). There was minimal to moderate inflammation (endometritis and/or myometritis) in 3/5 ZIKV-infected pregnancies while a fourth ZIKV dam, 664184, had a large uterine diverticulum (outpouching of the uterine wall) with severe segmental infarction, necrosuppurative inflammation, and ischemic necrosis, confounding interpretation of the stillbirth of (infant 416597) at 133 days (Table 2 and Fig 3). The placentas of 3/5 ZIKV-infected pregnancies had neutrophilic villitis. In summary, a

majority of the ZIKV-infected pregnancies had inflammation, with all ZIKV-infected pregnancies having either neutrophilic deciduitis, endometritis, myometritis or villitis.

Table 2. Histopathological description of decidua, placental bed and uterus, and placenta.

Tissue Source	Organ System	Tissue Name	ZIKV-exposed					Control
			Dam: 664184	Dam: 484880	Dam: 795784	Dam: 918724	Dam: 730267	Dam: 020101
			Fetus: 416597	Infant: 424847	Infant: 499874	Infant: 527421	Infant: 226691	Infant: 020501
Maternal	Reproductive	Decidua	Mild multifocal to diffuse neutrophilic deciduitis with multifocal necrosis.	Occasional rare aggregates of lymphocytes not diagnosed as deciduitis.	Mild multifocal lymphoplasmacytic to neutrophilic deciduitis. With Mild multifocal necrosis	Subacute to chronic lymphoplasmacytic deciduitis with multifocal necrosis and acute hemorrhages and mild-moderate, multifocal lymphoplasmacytic and neutrophilic vasculitis.	Moderate multifocal chronic lymphoplasmacytic and neutrophilic deciduitis.	Mild multifocal persistent muscularization of arteries and minimal multifocal chronic lymphoplasmacytic deciduitis.
		Uterine placental bed	Focally extensive uterine diverticulum with severe segmental ischemic necrosis, severe diffuse necrosuppurative myometritis and endometritis, with perivascular hemorrhage, and vascular thrombosis	Minimal multifocal lymphocytic myometritis and mild multifocal random and perivascular lymphocytic endometritis.	Minimal lymphocytic endometritis.	There are no significant histologic lesions.	Moderate multifocal lymphoplasmacytic, perivascular myometritis.	There are no significant histologic lesions.

Fetal	Extraembryonic	Placenta	Multifocal severe ischemic necrosis of villi with mild multifocal to diffuse deciduitis.	Moderate multifocal regional basal plate infarction, acute coagulative necrosis, with neutrophilic villitis and intervillositis.	Multiple chronic (remote) infarctions with neutrophilic villitis and intervillositis.	Severe multifocal necrotizing and neutrophilic villitis and intervillositis with multifocal villous loss and collapse.	Moderate, multifocal decidual and basal plate persistent muscularization of arteries with multifocal fibrinoid necrosis, moderate lymphoplasmacytic and occasional neutrophilic vasculitis, moderate multifocal distal villous hypoplasia	Retroplacental hemorrhage, moderate multifocal basal thrombosis with ischemia and infarction with minimal multifocal intervillous fibrin and syncytial knots, focal avascular villi, mild multifocal subchorionic fibrin

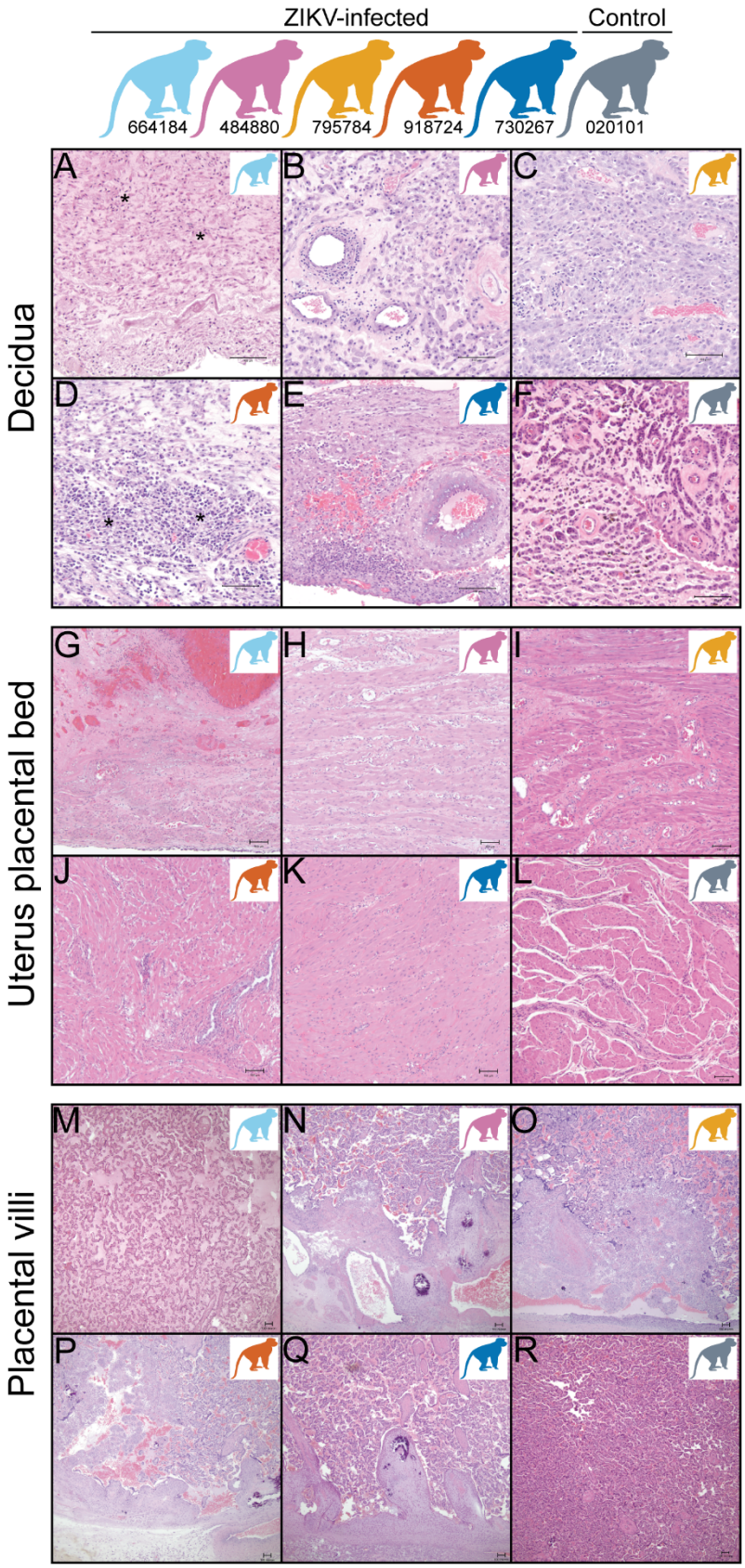

Figure 3. Decidua, placental bed and placental villous pathology.

ZIKV RNA was not detected by qRT-PCR in the uterine placental bed, uterus or vagina in ZIKV-exposed dams (Fig 4). The maternal-fetal interface tissues, including the placental discs, umbilical cord, amniotic/chorionic membrane were also negative in all the ZIKV-exposed dams. Only the decidua in 1 of 5 ZIKV-exposed animals (dam 795784) had detectable ZIKV RNA at 56 copies/mg. Because detection of vRNA can be focal, we also assessed other sections of the placenta, decidua and amniotic/chorionic membrane for ZIKV RNA by ISH. This complementary method of detecting ZIKV RNA identified additional positive tissues including the decidua, amniotic/chorionic membrane in pregnancy 664184/416597 (dam ID/fetus ID) (Fig 4). Thus, 2 of the 5 ZIKV-exposed pregnancies (one of which was the stillborn infant) had ZIKV RNA detected in the female reproductive tissues or in the extraembryonic tissues at the time of delivery.

A

Tissue Source	Tissue Name	Animal ID (dam ID/fetus-infant ID)									
		664184/416597		484880/424847		795784/499874		918724/527421		730267/226691	
		qRT-PCR	ISH	qRT-PCR	ISH	qRT-PCR	ISH	qRT-PCR	ISH	qRT-PCR	ISH
Maternal tissues	Decidua	0	positive	0	negative	56 copies vRNA/mg	negative	0	negative	0	negative
	Placental bed	0	NT	0	NT	0	NT	0	NT	0	NT
	Uterus	0	NT	0	NT	0	NT	0	NT	0	NT
	Vagina	0	NT	0	NT	0	NT	0	NT	0	NT
Fetal extraembryonic tissues	Amniotic/chorionic membrane	0	positive	0	negative	0	negative	0	negative	0	negative
	Placental disc 1	0	negative	0	negative	0	negative	0	negative	0	negative
	Placental disc 2	0	negative	0	negative	0	negative	0	negative	0	negative
	Umbilical cord	0	NT	0	NT	0	NT	0	NT	0	NT
	Amniotic fluid	NC	NA	0	NA	0	NA	0	NA	0	NA

B

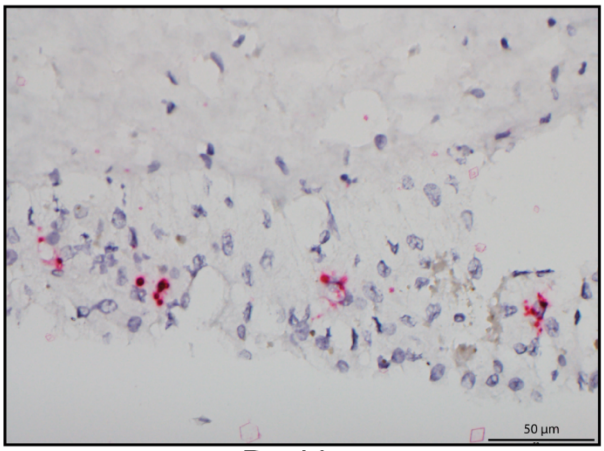

Decidua

C

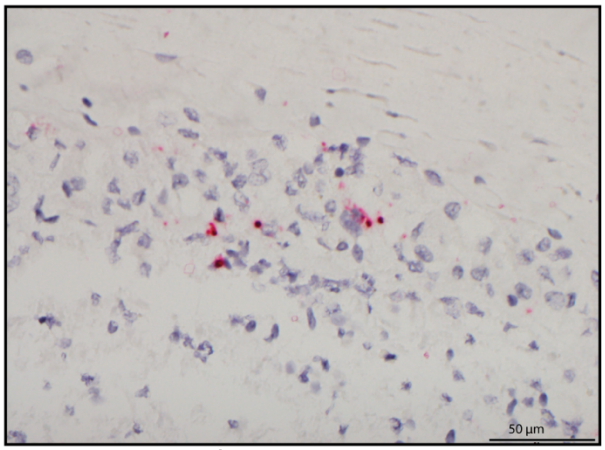

Amniotic/chorionic membrane

Figure 4. Viral loads and ISH in the maternal-fetal interface.

Infant clinical courses

ZIKV-exposed infants were delivered by Cesarean delivery at 154-155 gd (approximately 104-114 days after maternal ZIKV challenge), except for the fetal demise that occurred at 133 gd (87 days after maternal ZIKV challenge) (S1 table). Three of four ZIKV-exposed liveborn infants required respiratory support during resuscitation efforts after delivery, with the level of respiratory support ranging from ambient blow-by oxygen to noninvasive positive pressure ventilation (S2 table). Because most of the infants delivered by Cesarean section at the WNPRC are delivered after gd165, the proportion of infants that require respiratory support is not well defined around gd155 when our infants were delivered. Of the three infants that

required respiratory support in the delivery room (499874, 527421, 226691), only 499874 required additional respiratory support after initial stabilization. After resuscitation, all the liveborn ZIKV-exposed infants were reared in the nursery. A single ZIKV-exposed infant (499874) that required respiratory support for tachypnea and poor oxygenation was weaned off of oxygen by 20 hours of life, likely secondary to transient tachypnea. Chest radiographs showed no abnormalities in infant 499874 and this infant never had an elevated WBC, although leukopenia was noted on day of life (DOL) 4 (S3 table). However, this infant (499874) required additional respiratory support after a sedated ocular exam on DOL 5, which included 4 hours of ambient oxygen supplementation for poor oxygenation and tachypnea, suggesting an underlying pulmonary pathology. None of the other infants that received sedated ocular exams, brain imaging or hearing exams required respiratory support after recovering from anesthesia.

Infant growth and feeding

Dysphagia, or difficulty swallowing, is a feature in some human infants with congenital ZIKV infection (16, 17), and is thought to be secondary to the lack of swallowing coordination from brain damage, posture abnormalities and abnormalities of digestive tract motility (16). Dysphagia is problematic because it can lead to poor weight gain or to pulmonary infections from aspiration. To indirectly assess dysphagia in our neonatal macaques, we assessed formula feeding volumes and daily weight gain. We compared whether daily weight gain and formula feeding volumes in our ZIKV-exposed infants were different from comparably treated control infants. Four ZIKV-exposed infants were reared in the nursery from DOL 0 to DOL 8, one control infant was reared in the nursery from DOL 0 to DOL 8, and two control infants were reared in the nursery from DOL 1 to DOL 8 (after maternal rejection following birth) (S1 table). We compared the ZIKV-exposed and control infants' weight gain and feeding volumes using a linear mixed effects model with animal specific random effects to determine if there was a difference between groups, using gestational age at birth as a covariate in the analysis because

of the difference in ages of two of the three control infants (r17104 and r18076) from the ZIKV-exposed infants. The ZIKV-exposed infants had a lower cumulative feeding volume trajectory compared with control infants during their first week of life (Table 3 & Fig 5). The ZIKV-exposed infants also had a slower rate of weight gain than the control infants (Table 3 & Fig 5). Infant 499874's postnatal respiratory distress could theoretically contribute to poor cumulative feeding volumes, but a chi-square outlier and Dixon and Grubbs outlier tests test did not indicate the presence of an outlier for the slope estimates (p=0.2379). Together, these data indicate that the four ZIKV-exposed infants had lower cumulative feeding volume trajectories and slower weight gain over the first week of life compared with three control infants.

Table 3. Comparison of weight gain and feeding volumes between ZIKV-exposed and control infants.

	ZIKV Slope (95% CI)	Control Slope (95% CI)	p-value
Cumulative feeding volume	4.8 (4.4-5.3)	6.1 (5.2-7.0)	0.0138
Weight	-2.9 (-8.0-2.3)	10.8 (5.5-16.0)	<0.001

Confidence interval (CI).

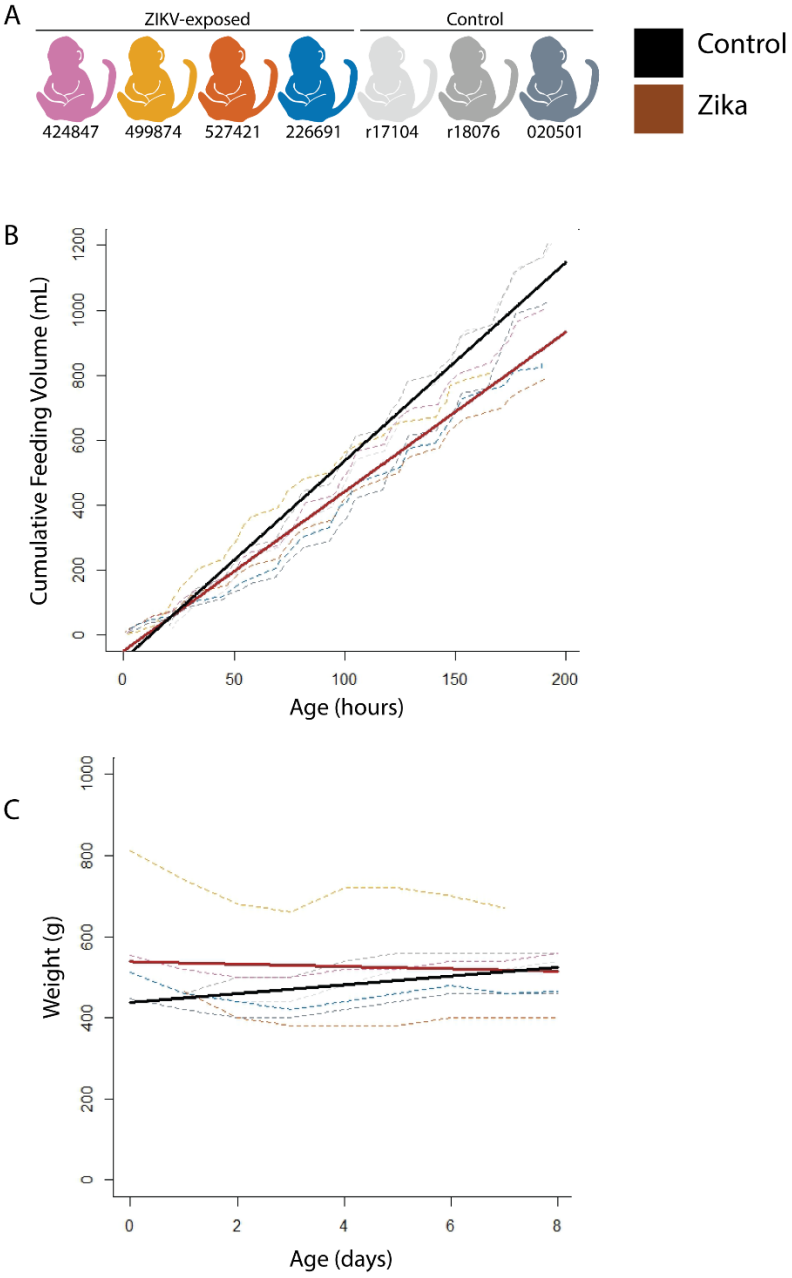

Figure 5. Infant weight gain and cumulative feeding volume.

Infant viral loads and antibody responses

Human infants with known exposure to ZIKV during pregnancy are recommended to have laboratory testing for ZIKV RNA and IgM in body fluids to confirm fetal infection, although these

tests have a number of limitations (6). ZIKV RNA is only transiently present in body fluids and IgM antibody levels may wane after infection (6). To determine if fetal infection could be confirmed in the four liveborn ZIKV-exposed infants, anti-ZIKV IgM responses were measured in serum using two different commercially-available assays. By both methods, all infant serum samples were negative for anti-ZIKV IgM (S4 figure). We also measured ZIKV RNA in infant body fluids (plasma, urine and CSF) during the first week of life by qRT-PCR to determine if fetal infection could be confirmed. Plasma, urine and CSF viral loads were negative in the ZIKV-exposed infants (S4 figure). We also measured neutralizing antibodies in infant serum by PRNT (S5 figure) and these demonstrated lower ED90 values compared with maternal PRNT ED90 values from the necropsy timepoint, indicating that the infants had overall lower neutralizing antibody titers compared with the dams at the closest available timepoint to the infant measurement. This infant neutralizing antibody titer likely represents transplacental transfer of IgG; assessments of infant serum months after birth, after maternal IgG has cleared, would have to be performed to determine the infant's contribution to the overall IgG titer.

Infant neurobehavioral development

Congenital ZIKV infection can result in neurodevelopmental delay in human infants (8, 18), so we sought to evaluate whether congenital ZIKV exposure in infant macaques results in neurobehavioral impairments. We evaluated neonatal macaques with a neurobehavioral assessment developed for rhesus macaques less than 1 month of age, termed the Schneider Neonatal Assessment for Primates (SNAP) (19, 20), which is based on the Brazelton Newborn Behavioral Assessment Scale (NBAS) (21). The SNAP has been validated to detect neurobehavioral impairments due to prenatal exposure to stress, alcohol, and lead in neonatal macaques (22-24). The SNAP assesses neonatal neurobehavioral development in four subscales, or constructs (motor maturity and activity, orientation, sensory and state control) (S4 table). We evaluated four ZIKV-exposed infants and one control infant that were all born at

similar gestational ages (154-157 gd) (S1 table) and reared in the nursery to match the conditions under which the infants were evaluated. Infants were evaluated on DOL 1 (ie ~24 hours after delivery; Trial 1), on days 3-5 of life (Trial 2), and on days 6-7 of life (Trial 3) (S1 table). There are no clear trends where the ZIKV-exposed infants as a group appear to differ from the single control infant, but given the small control sample size of a single animal, no definitive comparisons can be made (Fig 6). While there is normative data published previously, these data did not match our infant population closely enough to be useful as a comparator in our SNAP evaluations (19, 20). Future work will increase the number of control infants in these assessments to enable a robust comparison of ZIKV-exposed and control infants; we include this data here to provide a foundation for these future analyses.

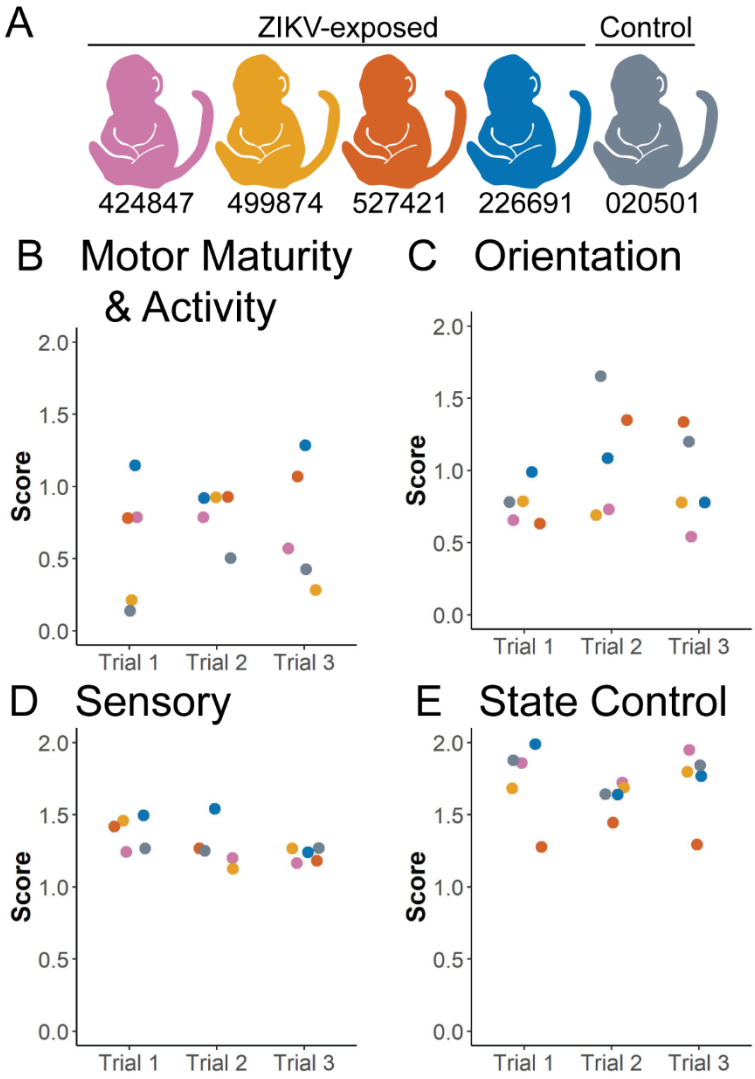

Figure 6. Neonatal neurobehavioral assessment.

Infant vision and hearing evaluation

The ocular system is affected in up to 88% infants with microcephaly with confirmed congenital ZIKV infection (25), though how often the ocular system is affected in ZIKV-exposed infants without microcephaly remains undefined. To determine whether the four liveborn ZIKV-exposed infants had signs of ocular malformations or visual system dysfunction, we performed fundoscopic ophthalmic exams, optical coherence tomography, and visual electrophysiology

studies. Four liveborn ZIKV-exposed infants were evaluated on either DOL 2 or 5 and two control infants from the breeding colony were assessed on DOL 7 or 13 for comparison for each of the ocular studies. Ophthalmic examination revealed minor, not clinically significant, defects in 2 of the ZIKV-exposed infants (S5 table), which included a corneal defect in one ZIKV-exposed infant (424847) and retinal pigmented epithelium mottling in another ZIKV-exposed infant (499874). No other corneal or retinal pigmented epithelium mottling defects were found in the other ZIKV-exposed infants or in the control infants. Intraocular pressures ranged from 6-14 mm Hg bilaterally in all the infants (S5 table). It is unknown whether these intraocular pressures are normal because there are no published intraocular pressures in neonatal macaques; only juvenile macaques (aged 7 months to 3 years) have been studied and they have an average intraocular pressure of 15.7 mm Hg (26). No optic nerve hypoplasia, choroidal lesions, lens abnormalities or vitreous opacities were identified in any of the infants evaluated. Portions of the intraocular blood system, the hyaloid artery and tunica vasculosa lentis, were identified in the ZIKV-exposed and control infants evaluated at the age of 7 days or less, with the 13-day-old infant having only a remnant hyaloid artery and still a persistent tunica vasculosa lentis. The persistence of the tunica vasculosa lentis is a normal finding in newborn rhesus macaques (27) at corrected gestational ages close to the infants used in these ocular exams. A persistent hyaloid artery in newborn rhesus macaques is a normal finding and typically persists until the age of 2-3 weeks (28).

Next, we evaluated the anterior segment of the eye and the retina by spectral domain optical coherence tomography (SD-OCT) to determine if there were differences between the ZIKV-exposed and control infants that were not apparent with ophthalmic exam. OCT uses non-invasive light waves to evaluate the anterior segment of the eye (ie the ocular structures anterior to the vitreous) and the retina. We assessed total retinal thickness, choroidal thickness and central corneal thickness, in addition to specific retinal layers described in Figure 7. There were

no significant differences between the total thickness of the retina, choroid and central cornea in ZIKV-exposed infants and controls (S6 table). Within the retina, there were differences between the thickness of the inner plexiform layer, outer nuclear layer, photoreceptor outer segment, and retinal nerve fiber layer between the ZIKV-exposed and control infants (S6 table), even after correcting for the slight differences between groups in regards to their age. There are age-related changes in layer thicknesses in both the outer nuclear layer and photoreceptor layers, as they get thicker from infancy to adulthood (29). Younger infants typically have persistent inner retinal layers (which includes the inner plexiform layer) which get thinner with aging (29), so it may be possible that the comparatively younger ZIKV-exposed infant group had a thicker inner plexiform layer simply due to a younger corrected gestational age at birth. However, we identified these quantitative differences in retinal layer thicknesses even after controlling for corrected gestational age. Additional studies are evaluating the contribution of prenatal ZIKV exposure and animals' specific age to these layer thicknesses.

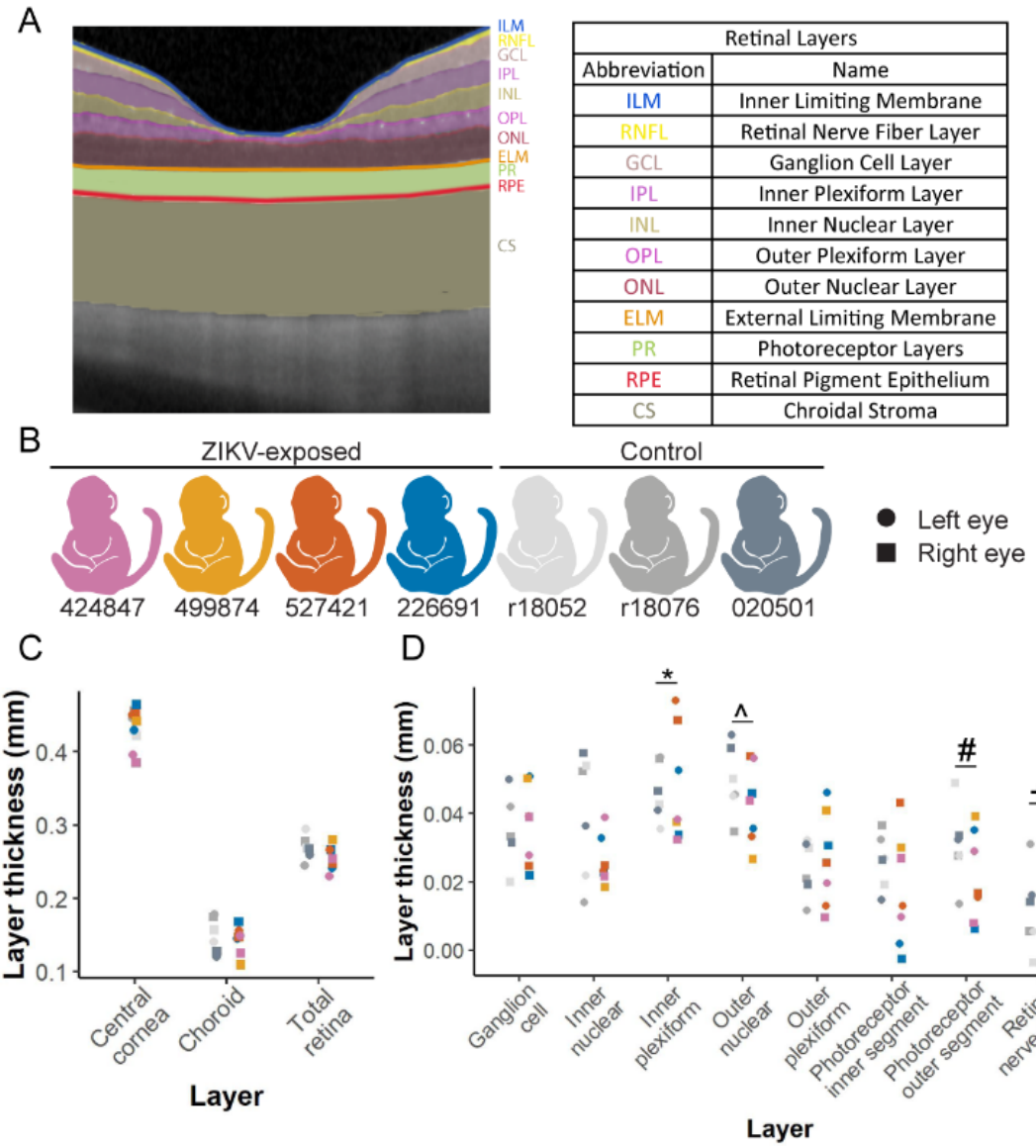

Retinal Layers	
Abbreviation	Name
ILM	Inner Limiting Membrane
RNFL	Retinal Nerve Fiber Layer
GCL	Ganglion Cell Layer
IPL	Inner Plexiform Layer
INL	Inner Nuclear Layer
OPL	Outer Plexiform Layer
ONL	Outer Nuclear Layer
ELM	External Limiting Membrane
PR	Photoreceptor Layers
RPE	Retinal Pigment Epithelium
CS	Chroidal Stroma

Figure 7. Retinal and choroidal layer thicknesses measured by optical coherence tomography.

To objectively evaluate visual function in ZIKV-exposed neonatal rhesus macaques, we performed standard visual electrodiagnostic procedures including a full-field electroretinogram (ERG) and the cortical-derived visual evoked potential (VEP) (30). The light-adapted (LA) full-field flash ERG, recorded on a rod-saturating background, measures the electrical activity generated by predominantly by cone photoreceptor and bipolar cells, which are found in high

density in the primate macula and are primarily responsible for light-adapted, high acuity and color vision. The ERG is used clinically to assess generalized retinal function under light-adapted (focused on cone photoreceptors) and dark-adapted (focused on rod photoreceptors) conditions (30) and has been used to characterize maculopathy in acute ZIKV infection (31). The VEP reflects the function of the entire visual pathway from the retina via the optic nerve to the visual cortex of the brain (30). We performed standard LA ERGs to measure how the cone photoreceptors function; these cone photoreceptors are primarily responsible for light-adapted, high acuity and color vision and are concentrated in the macula. When controlling for the small differences between the infant's corrected gestational ages at the time of the ocular exam, the only statistically significant difference identified in the visual electrophysiology studies was within the LA ERG, and specifically within the A wave latency of the left eye (Fig 8 and S7 table). The A wave represents how well the rod and cone photoreceptors within the outer photoreceptor layer in the retina are functioning. In comparison, the VEP did not identify any statistically significant differences between the groups (S7 table), suggesting that the optic pathway between the retina and occipital cortex is functioning at a similar level in both groups.

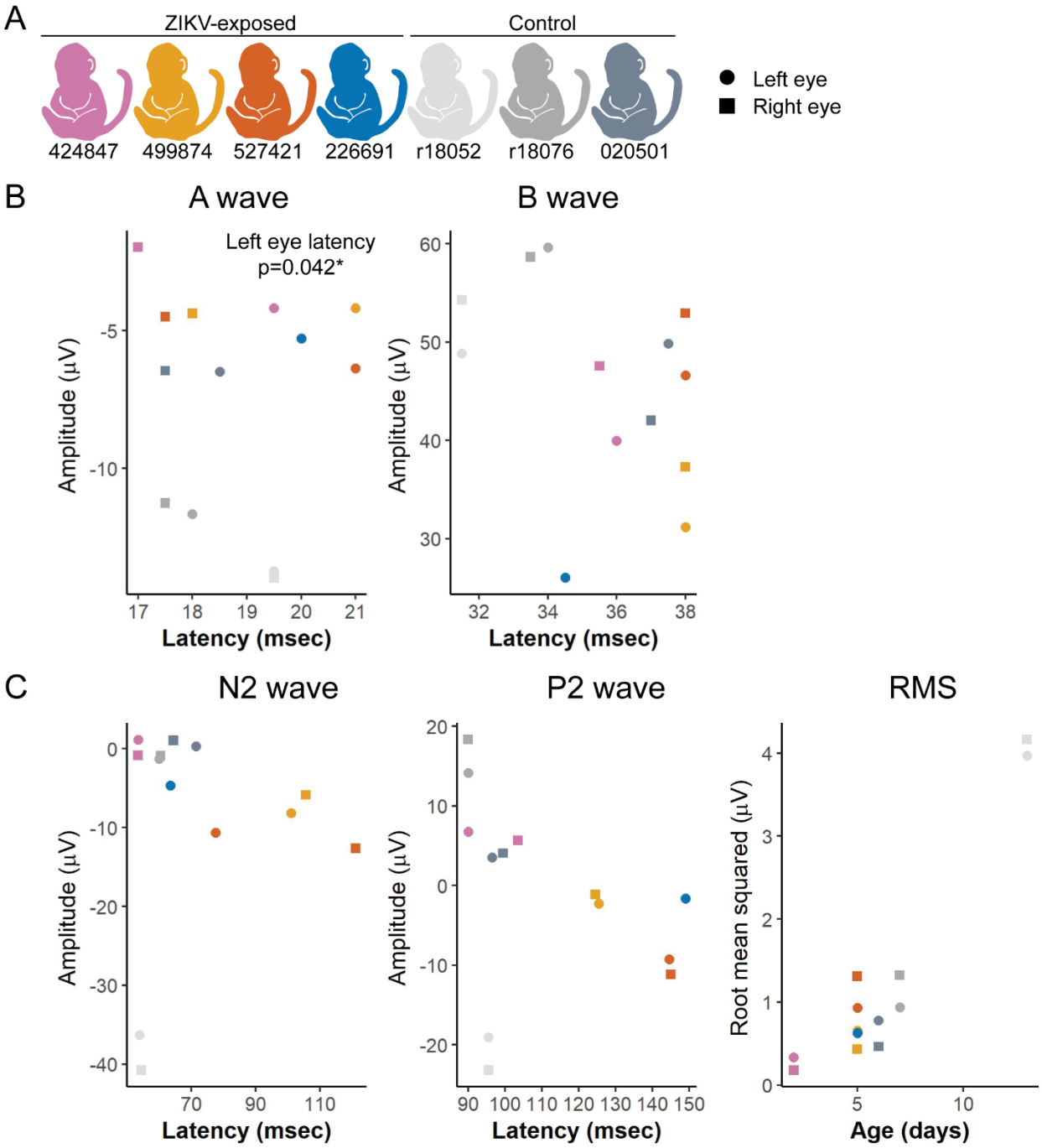

Figure 8. Electroretinography and visual evoked potentials.

We also evaluated hearing in these macaque infants because human infants with confirmed ZIKV infection have a 4.3% incidence of hearing loss (32) and hearing tests are one of the

recommended evaluations for infants with known maternal ZIKV infection during pregnancy (6). We sought to determine whether the ZIKV-exposed infants in this study had evidence of hearing loss with auditory brain response (ABR) testing, which is a common method of assessing hearing by measuring the brainstem's electrical activity (measured as waveforms) in response to auditory stimuli (clicks) in people or animals who cannot communicate auditory responses and cannot complete a typical behavioral audiological evaluation. We obtained measurable ABR thresholds to click stimuli in one of the ZIKV-exposed liveborn infants (226691) and compared it to ABR thresholds in two control infants that were not exposed to ZIKV in utero (r17104 and 020501). The ZIKV-exposed infant underwent the exam at 5 days of age and had present responses to click stimuli at all levels tested (70, 50, and 30 dB nHL) in the right and left ears (S6 figure), indicating that this infant had brainstem responses to click stimuli at multiple sound intensities. Due to equipment availability, the procedure was only able to be done on one ZIKV-exposed infant. Because the ZIKV-exposed infant and control infants were different ages at the time of the ABR testing (DOL 5 and 84, respectively), subtle differences in latency times cannot be compared robustly. While ABRs are commonly done in adult macaques (33), they are not commonly done in infant macaques (34) and no published normative values exist. We hope to increase the publicly available normative data for ABRs in infant macaques by describing our values even though we did not have a large enough sample size to make robust comparisons between ZIKV-exposed and control groups. Future studies with age-matched controls will evaluate hearing in this macaque model of congenital infection more robustly.

Infant brain imaging

Up to 17% of fetuses with documented maternal ZIKV infection in utero have central nervous system (CNS) anomalies in some studies (35). As a result, cranial ultrasonography after birth is recommended for human infants with findings consistent with CZS after birth (6). We sought to characterize brain anomalies that would not necessarily be visualized with cranial

ultrasonography or CT scan, and instead performed brain MRIs on all the liveborn ZIKV-exposed infants (n=4). In these four ZIKV-exposed infants, no severe brain abnormalities including subcortical calcifications, ventriculomegaly, cortical thinning, gyral pattern anomalies, cerebellar hypoplasia or corpus callosum anomalies were identified on qualitative neuroradiological interpretation. To evaluate for subtle changes that would not be apparent on qualitative neuroradiological interpretation, we used voxel-based morphometry (VBM) to objectively compare the grey matter volume and density of entire brain regions between ZIKV-exposed infant brains and controls. A voxel is a three-dimensional pixel and is the basic unit within medical scans, used to measure signal that in a Bravo scan relates to grey vs white matter. VBM is an objective approach that enables a voxel-wise estimation of the local amount of a specific tissue (36) and has been used successfully to identify reduced grey matter volumes in human children with autism (37). In this VBM comparison, we compared 4 ZIKV-exposed infant brains to 13 healthy control infant T1 MRI brain images (S1 table) using a VBM computational comparison approach entitled Data Processing and Analysis for Brain Imaging (DPABI) (38) using age and sex as covariates. We identified two regions located in the precentral and superior frontal gyrus where the volume and density of grey matter differed between ZIKV-exposed infants and control infants (uncorrected $p < .001$) (Fig 9A-B). In these regions, the ZIKV-exposed infant brains had a greater volume and higher density of grey matter. These differences were not apparent in the clinical neuroradiologic interpretations and were only detected by VBM comparisons (Fig 9C). In summary, we identified grey matter volume and density abnormalities within the precentral and superior frontal gyrus in the ZIKV-exposed brains, providing target locations for neuropathological assessments in future studies and suggesting that in utero ZIKV exposure may result in grey matter abnormalities which are found in many neurologic and psychiatric diseases (39-41).

A

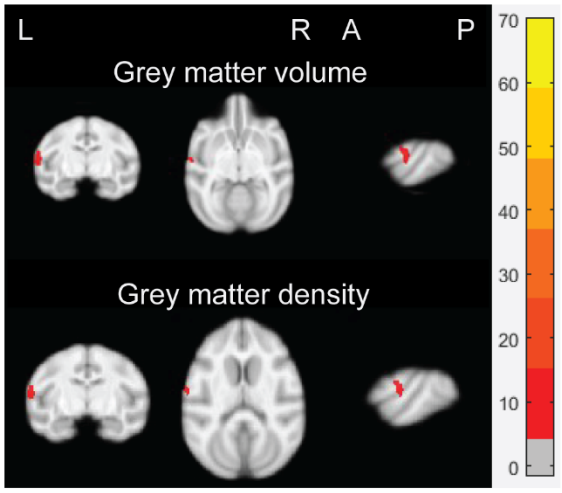

B

Regions	Stereotaxic coordinates			*t-value*
	x	*y*	*z*	
Gray matter volume				
Left precentral gyrus	-27	14	14	5.162
Left superior frontal gyrus	-27	14	19	4.925
Gray matter density				
Left precentral gyrus	-26	14	15	5.143
Left superior frontal gyrus	-26	15	20	4.611

C

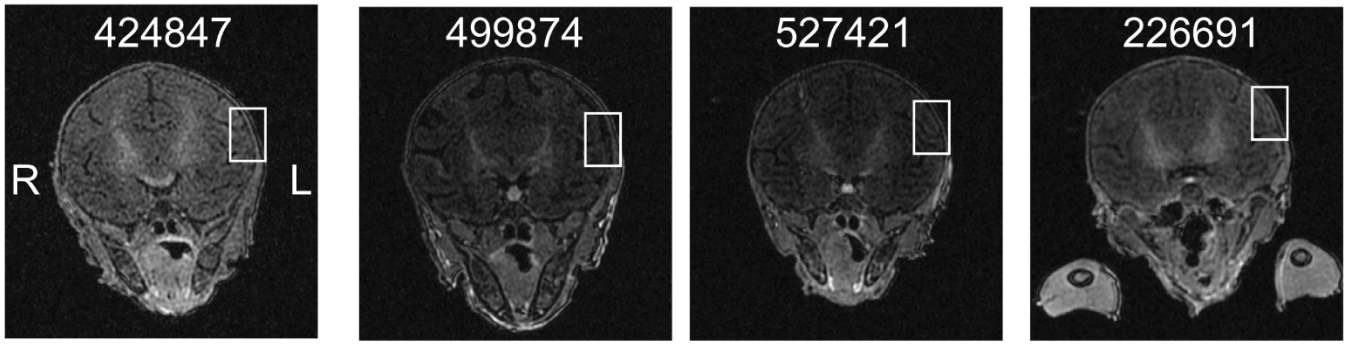

Figure 9. MRI analysis and voxel-based morphometry comparison.

Infant tissue histopathology and vRNA distribution

In order to define ZIKV tissue distribution, tissue pathology and attempt to confirm fetal infection, the ZIKV-exposed liveborn infants (n=4) were euthanized and submitted for necropsy on day of life 7-8 (Fig 10). The gd133 stillborn fetus (416597) was submitted for necropsy immediately after delivery. One liveborn infant (020501) was euthanized on DOL 8 a control for histopathology (S1 table). To compare whether gross size differences existed between the ZIKV-exposed infants and the control infant, we obtained detailed morphometric measurements on all the ZIKV-exposed fetuses/infants (except for 499874 where measurements were not done). The measurements of the control infant were within range of the measurements of the 3

age-matched ZIKV-exposed infants (S8 table). It is challenging to determine whether the ZIKV-exposed infants has microcephaly postnatally because there are no standardized growth curves for macaque infants born at a gestational age of 155 days. The closest reference ranges come from a study where the infant's gestational age was not described, but may be presumed to be at least 165gd because no surgical delivery is described (42), and our macaque infant's morphometric measurements are comparably smaller than these published measurements. The fetal demise case has notably smaller measurements than the other ZIKV-exposed infants and the control infant, likely representing its younger gestational age rather than a growth restriction because its growth parameters as measured on ultrasonography (Fig 2 and S2 figure) were not outside the range of +/- 2 SD.

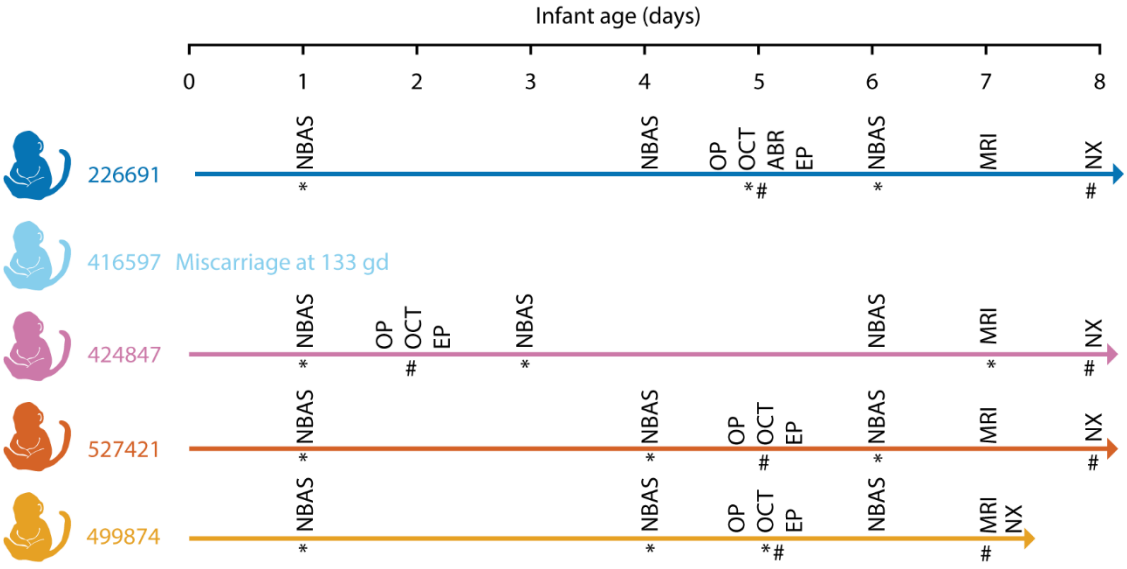

Figure 10. ZIKV-exposed infant examination schedule.

In order to identify tissue damage associated with ZIKV exposure in utero, approximately 48 tissues were evaluated for each infant/fetus. The consistent histologic findings of the ZIKV-exposed fetus/infants included neutrophilic otitis media in 3 of 5 ZIKV-exposed fetuses/infants (Fig 11), bronchopneumonia in 2 of 5 ZIKV-exposed infants, neutrophilic lymphadenitis in 3 of 5

ZIKV-exposed infants (Table 4 and Fig 12). The infant who had respiratory distress after birth and with each sedation event (499874) had bronchopneumonia identified by histopathology; the other infant with histological bronchopneumonia (226691) had no respiratory symptoms. There were no lesions identified by hematoxylin and eosin (HE) staining in the eye or CNS tissues of any of the ZIKV-exposed infants or in the control infant; additionally, no remaining tissues had lesions that affected more than one fetus/infant. HE stained brains had no significant histologic lesions; additional staining and quantitative analyses are in progress. The prenatal ultrasound findings of pericardial effusions and hepatic hyperechoic regions were not identified by histopathology (S3 figure). The full list of evaluated tissues not identified as abnormal in >1 infant is defined in Table S9.

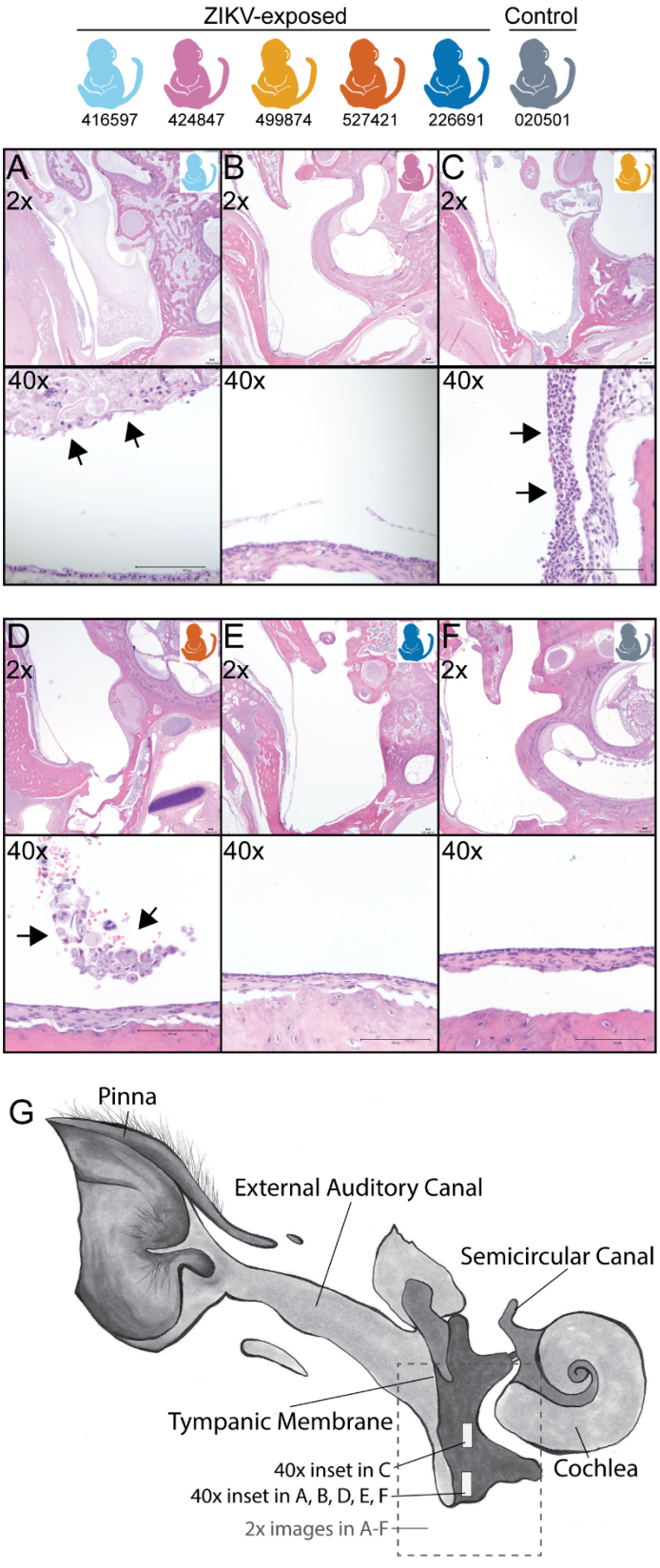

Figure 11. Fetus/Infant tissue histopathology of the ear.

Table 4. Histopathological description of the lymph nodes, lung and middle ear in fetuses/infants.

Tissue Source	Organ System	Tissue Name	ZIKV-exposed					Control
			Fetus: 416597	Infant: 424847	Infant: 499874	Infant: 527421	Infant: 226691	Infant: 020501
Fetus/infant	Immune	Mesenteric LN	NC	Minimal neutrophilic lymphadenitis with hemosiderosis	No significant lesions	No significant lesions	No significant lesions	Minimal neutrophilic inflammation with hemosiderosis
		Tracheobronchial LN	Moderate to severe diffuse autolysis with no other significant lesions.	No significant lesions	Moderate to marked neutrophilic lymphadenitis	NC	Minimal neutrophilic lymphadenitis.	Mild neutrophilic lymphadenitis
	Pulmonary	Lung	Moderate autolysis, moderate diffuse atelectasis, moderate numbers of squamous cells within alveoli, and variable amounts of cellular debris, consistent with dystocia and fetal	No significant lesions	Moderate to marked, multifocal, lymphoplasmacytic and neutrophilic interstitial pneumonia with moderate, multifocal, neutrophilic and necrotizing interstitial bronchiolitis.	Mild diffuse perivascular edema surrounding large pulmonary arteries.	Severe diffuse bilateral neutrophilic bronchopneumonia with atelectasis. Bacteria were not identified.	Small numbers of alveolar macrophages throughout alveoli. Occasional macrophages exhibit erythrophagocytosis and there are rare plasma cells within alveoli as well. A rare syncytial cell

			distress in utero. Bacteria were not identified.		Bacteria were not identified.			(multinucleated) is noted.
	Ear	Ear	Left ear: Minimal neutrophilic otitis media with intraluminal squamous cells. Bacteria were not identified. Right ear: Minimal neutrophilic otitis media with intraluminal squamous cells.	No significant histologic lesions bilaterally	Moderate to marked subacute neutrophilic otitis media. Bacteria were not identified.	Left ear: Minimal neutrophilic otitis media. Bacteria not identified. Right ear: no significant histologic lesions	No significant histologic lesions bilaterally	No significant histologic lesions bilaterally

Lymph node (LN). Not collected (NC).

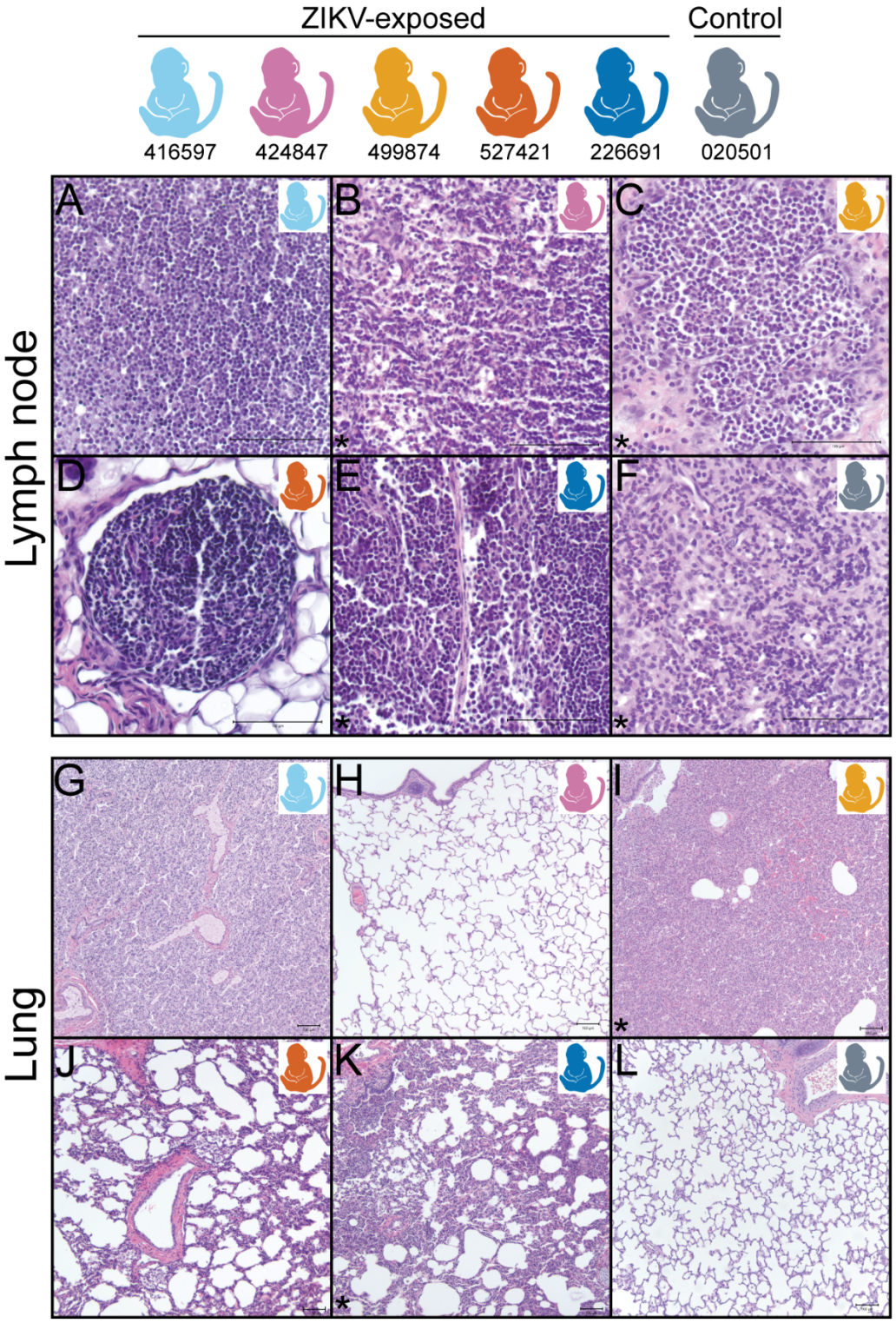

Figure 12. Fetus/Infant tissue histopathology of the lymph node and lung.

No ZIKV vRNA was identified by qRT-PCR in over 45 tissues and body fluids examined per infant/fetus at necropsy (S10 table), including multiple brain sections. Brain sections were also examined by in situ hybridization (ISH) for ZIKV RNA to assess different brain sections for ZIKV RNA than had been evaluated by qRT-PCR, and there no positive staining in any of the fetus/infant brain sections evaluated (S8 figure). We also searched for ZIKV RNA by ISH of the infant/fetus lung tissue, as this tissue had high viral loads in our previous studies (43), and in the cochlea, because of the clinical findings of sensorineural hearing loss in human congenital ZIKV infection, but no fetal/infant lung or cochlea section had positive ZIKV ISH.

Discussion

We identified neurodevelopmental changes in ZIKV-exposed macaque infants without evidence of vertical transmission. The finding of decreased feeding volumes and slower weight gain in this macaque model is important given the finding of dysphagia in human infants with CZS (16) and how significantly dysphagia affects overall functional outcomes in children with neurodevelopmental deficits (44). The differences between our ZIKV-exposed and control group feeding volumes and weight gains existed even while controlling for the differences in gestational ages at birth between the groups and evaluating whether the presence of an infant with respiratory distress in the ZIKV-exposed group affected the overall group feeding volumes. This suggests that clinicians should pay close attention to weight gain and dysphagia in infants with prenatal ZIKV exposure, not just with apparent CZS, and that future studies of congenital ZIKV exposure in macaque models should continue to evaluate these measurements as a marker of long-term functional outcome.

We were interested in determining whether the ZIKV-exposed infants had evidence of morphological changes in brain, particularly in regions related to feeding functions. Indeed, we identified differences in a region of the brain involved in swallowing, the pharyngeal motor cortex (45), in quantitative grey matter analyses. The grey matter volume and density changes in the precental and superior frontal gyrus (the pharyngeal motor cortex region) were not identified by qualitative neuroradiologic assessment, but rather by quantitative voxel-based morphometric (VBM) comparison. We did not identify brain anomalies typically present in infants with CZS by qualitative neuroradiologic assessment of the brain MRIs, including cerebral cortex thinning, abnormal gyral patterns, ventriculomegaly, calcifications or cerebellar hypoplasia (46). The ZIKV-exposed infants had a larger grey matter volume and density even when controlling for slight differences in ages between the ZIKV-exposed and control groups. While identifying this difference solely on the left side of the brain is unexpected, this difference may be due to our small sample size. Abnormalities in grey matter measurements have been associated with many neurologic and psychiatric diseases, including neurodegenerative disorders, autism spectrum disorders and epilepsy (39-41, 47-49). Normal brain development processes in the postnatal period may also play a role in this finding of increased grey matter volume and density. Normally, grey matter volume increases rapidly in infancy with an overproduction of neural and glial cells, neural processes and synapses followed by gradual pruning (50). Increased grey matter volume and density in the ZIKV-exposed infants suggests that one or more of these developmental processes has been altered. While it is impossible to describe histopathological changes based on MRI, we can hypothesize that there may be abnormal cortical neuronal migration that results in increased neuron density in some cortical regions and decreased density in others, and this is supported by the finding of neuronal migration disorders in human congenital ZIKV infection (51). There was no histological-MRI correlation when examining HE stained sections of ZIKV-exposed infant brains because no abnormalities were

identified. Quantitative studies evaluating specific cell populations are underway to define the histological etiology of these grey matter abnormalities in the ZIKV-exposed infant brains.

We confirmed maternal ZIKV infection in all five dams inoculated with ZIKV in the first trimester and confirmed seroconversion by 28 dpi in the dams. Despite this confirmed maternal infection, we were not able to confirm ZIKV transmission to the fetus/infant at the time of delivery or at necropsy (7-8 days of age) because of the absence of ZIKV RNA in fetal/infant tissues or body fluids. The infants also had no detectable ZIKV-specific IgM response. The lack of evidence of vertical transmission is a well-defined limitation in the study of infants born to mothers with documented ZIKV infection during pregnancy (6), which is why human clinical trials characterizing long term outcomes of children born to women with documented or suspected ZIKV infection during pregnancy do not require proof of ZIKV RNA in infant body fluids or ZIKV-specific IgM in infant serum for enrollment (52-54). Better diagnostic tools need to be developed to evaluate for fetal infection months after maternal ZIKV infection.

Ocular anatomic structures also differed significantly between the ZIKV-exposed and control infants. As with the qualitative brain imaging approach described above, with a qualitative ophthalmic exam we did not identify any anterior or posterior segment abnormalities. Only with a quantitative evaluation by OCT were we able to identify differences between ZIKV-exposed infants and control infants. In our quantitative OCT analysis, there were four layers of the retina where ZIKV-exposed infants had significantly different thicknesses compared with the control infants even when controlling for age. Although a younger average age of the ZIKV-exposed infant group could explain the thinner outer nuclear layer and photoreceptor segment layer thicknesses (29), along with the thicker inner plexiform layer (29), these differences were present even though we controlled for age. Another hypothesis for the thinner photoreceptor outer segment and outer nuclear layer between the ZIKV-exposed and control groups is that

this outer segment of the retina is more sensitive to decreased oxygen levels because the partial pressure of oxygen is lowest in these outer segments (55). Any in utero stressors that would decrease oxygen levels, including placental dysfunction as described in another macaque model of ZIKV infection (56), could affect these layers of the retina more than other layers. As no histological abnormalities were noted on HE evaluation of the retinal layers, further studies evaluating the association between outer retinal layer thicknesses and the degree of placental pathology are underway.

Quantitative analysis of the visual pathways using visual electrophysiology studies also identified differences between the ZIKV-exposed and control infants which was not apparent on qualitative ophthalmic exams. When comparing the visual neural pathways, we found a difference in the photopic ERG, which measures the light-adapted electrical response in the retinal cone photoreceptors and postsynaptic bipolar cells, even when controlling for age. The A wave is derived from the rods and cones of the outer photoreceptor layer, which corresponds to the thinner photoreceptor outer segment in ZIKV-exposed infants seen in the OCT analysis. This suggests that the early stages of retinal neural activity, including the retinal visual cycle, the phototransduction cascade, and glutaminergic activation of on- and off- bipolar cells are affected by prenatal ZIKV exposure. In comparison, when we evaluated the function of the visual neural pathway from the retina to the visual cortex, we noted no significant differences between the ZIKV-exposed infants compared with control infants. Human congenital ZIKV infection results in retinal abnormalities and a thinned photoreceptor layer is one of the abnormalities described (57), so our macaque model accurately models what is found in human ZIKV infection and identifies it within the first week of life. In murine models of ZIKV infection, photoreceptor loss is thought to occur secondary to compromised neural support by Müller cells and the retinal pigmented epithelium, which are preferentially infected by ZIKV (58). Because we did not identify qualitative abnormalities in the retinal layer histology by HE evaluation, quantitative

analyses of these regions to evaluate the numbers of specific cell types remaining after prenatal ZIKV infection are planned.

The ultimate goal of combining histopathology and comprehensive infant clinical evaluations in a macaque model of congenital ZIKV infection is to correlate qualitative and quantitative outcomes with tissue histopathology, better define mechanisms of disease, and develop preventive and therapeutic interventions. In these studies, histopathology of the maternal-fetal interface identified inflammation, specifically neutrophilic deciduitis, lymphoplasmacytic myometritis and endometritis, and villitis in the decidua, uterine bed and placenta, respectively, in the majority of the ZIKV-exposed pregnancies. Neutrophilic inflammation is not a new finding in ZIKV infection in pregnancy and it has been previously identified in the decidua (59, 60), chorion and amniotic membranes (60, 61) and placenta (60, 61) in macaque models, and in fact, uteroplacental pathology can lead to placental dysfunction and impairs transplacental transport of oxygen to the fetal compartment (56). One of the hypotheses for why posterior segments of the retina (which includes the retinal nerve fiber layer and inner plexiform layer) had different thickness between our ZIKV-exposed and control infants is because those layers are particularly sensitive to decreased oxygen levels (55), and the uteroplacental pathology we observed could lead to placental dysfunction and hypoperfusion of oxygen to the fetal compartment.

Our histopathological evaluations identified neutrophilic inflammation (otitis media, lymphadenitis and bronchopneumonia) in the ZIKV-exposed fetus and infants. Pulmonary neutrophilic inflammation is not a new finding in macaque fetuses affected by congenital ZIKV infection, as it has been previously identified in fetal lungs (43), but the finding of otitis media and lymphadenitis, was unexpected. Otitis media in the neonatal period is not common in human or macaque infants, though it can occasionally present as an isolated infection or as part

of septicemia (62). While congenital ZIKV infection is associated with hearing loss (32), this is the first report of otitis media in ZIKV-exposed macaque infants. Otitis media is a relatively uncommon finding in the neonatal period and in human neonates is found in only 4% of infants between 0-2 weeks of age (63). The prevalence of otitis media in rhesus macaque neonates is not defined. Congenital ZIKV infection in humans has also not been associated with lymphadenitis or pneumonia in the neonatal period, but has been associated with lung disease secondary to dysphagia in later infancy (~18 months of age) (64), so our findings of bronchopneumonia, otitis media and lymphadenitis may be incidental findings seen in our macaque infants that would not have been identified in human infants that do not undergo complete necropsies with histopathological evaluation, or may be clues that neutrophilic inflammation is more exuberant in ZIKV-exposed infants and these types of diseases should be evaluated for carefully in human infant cohort studies. We did not have a large enough sample size to assess whether our infants with otitis media had decreased hearing compared with control infants, but future hearing tests performed longitudinally in this macaque model should carefully evaluate for sensorineural and conductive hearing loss.

In summary, we describe the first qualitative and quantitative analysis of birth defects and neurodevelopment in a macaque model following exposure to ZIKV during pregnancy, and highlight areas of differences between ZIKV-exposed infants and controls that warrant close evaluation in future longitudinal macaque and human cohort studies. Our case series highlights the range of outcomes present in this macaque model of congenital ZIKV exposure, from fetal demise and bronchopneumonia, to grey matter abnormalities, dysphagia and visual pathway abnormalities. Future longitudinal studies in macaque models should, at a minimum, conduct qualitative assessments that are performed in longitudinal human cohort studies, including hearing tests, brain imaging, neurodevelopmental assessments and ophthalmic exams. However, future macaque models should also focus on the quantitative evaluations like the

ones we performed in this study, the ocular studies (OCT and visual electrophysiology studies) and brain MRIs (voxel-based morphometric comparisons). Correlating results from these quantitative assessments done in infancy with longitudinal studies of neurodevelopment throughout the juvenile years may enable macaque models to help predict which infants with prenatal ZIKV exposure are at the highest risk for neurodevelopmental deficits that only become apparent later in childhood.

Early identification of neurodevelopmental deficits, and early intervention with targeted therapies, are key to maximizing the functional potential of children (65). Human cohort studies have only recently identified that up to one third of asymptomatic infants without CZS have neurodevelopmental deficits apparent in the second year of life (9, 10). Because infants born during the peak of the American ZIKV epidemic in 2016 (66) are reaching preschool ages now and cohort studies of these children are still in progress, we have yet to learn whether an even greater number of children will have neurodevelopmental deficits that affect their functional outcomes in elementary school and beyond. Because macaques develop at an accelerated rate compared with humans, longitudinal studies performed with this macaque model focusing on correlating functional outcomes (social, motor, sensory) with specific neural pathways and anatomic structures identified in early infancy, can complement longitudinal human cohort studies by enabling clinicians to identify high risk children early and enroll them in targeted therapies. Many of these quantitative assessments will not be available in ongoing human cohort studies because they are costly, invasive and time-consuming, and so complementing large human cohort studies with smaller macaque model studies will help drive the basic understanding of which infants will develop neurodevelopmental deficits later in childhood.

Methods

Study Design

Indian-origin rhesus macaques (*Macaca mulatta*) were inoculated with Zika virus (see below for details) during the first trimester (term 165±10 days) (Table 1). These macaques were part of the Specific Pathogen Free (SPF) colony at the Wisconsin National Primate Research Center (WNPRC) and were free of *Macacine herpesvirus 1* (Herpes B), simian retrovirus type D (SRV), simian T-lymphotropic virus type 1 (STLV), and simian immunodeficiency virus (SIV).

Ethics Statement

All monkeys are cared for by the staff at the WNPRC in accordance with the regulations and guidelines outlined in the Animal Welfare Act and the Guide for the Care and Use of Laboratory Animals, the recommendations of the Weatherall report (https://royalsociety.org/topics-policy/publications/2006/weatherall-report), and the principles described in the National Research Council's Guide for the Care and Use of Laboratory Animals. The University of Wisconsin - Madison, College of Letters and Science and Vice Chancellor for Research and Graduate Education Centers Institutional Animal Care and Use Committee approved the nonhuman primate research covered under protocol number G005401-R01. The University of Wisconsin - Madison Institutional Biosafety Committee approved this work under protocol number B00000117.

Care & Use of Macaques

All animals were housed in enclosures with required floor space and fed using a nutritional plan based on recommendations published by the National Research Council. Dams were fed a fixed formula, extruded dry diet with adequate carbohydrate, energy, fat, fiber, mineral, protein, and vitamin content. Macaque dry diets were supplemented with fruits, vegetables, and other edible objects (e.g., nuts, cereals, seed mixtures, yogurt, peanut butter, popcorn, marshmallows, etc.) to provide variety to the diet and to inspire species-specific behaviors such as foraging. Infants were fed 5% dextrose for the first 24 hours of life and liquid formula subsequently. To further

promote psychological well-being, animals were provided with food enrichment, structural enrichment, and/or manipulanda. Environmental enrichment objects were selected to minimize chances of pathogen transmission from one animal to another and from animals to care staff. While on study, all animals were evaluated by trained animal care staff at least twice each day for signs of pain, distress, and illness by observing appetite, stool quality, activity level, physical condition. Animals exhibiting abnormal presentation for any of these clinical parameters were provided appropriate care by attending veterinarians. Prior to all minor/brief experimental procedures, macaques were sedated using ketamine anesthesia and monitored regularly until fully recovered from anesthesia.

The female macaques described in this report were co-housed with a compatible male and observed daily for menses and breeding. Pregnancy was detected by ultrasound examination of the uterus at approximately 20-24 gestation days (gd) following the predicted day of ovulation. The gd was estimated (+/- 2 days) based on the dam's menstrual cycle, observation of copulation, and the greatest length of the fetus at initial ultrasound examination which was compared to normative growth data in this species (67). For physical examinations, virus inoculations, some ultrasound examinations, blood and swab collections, the dam was anesthetized with an intramuscular dose of ketamine (10 mg/kg). Blood samples from the femoral or saphenous vein were obtained using a vacutainer system or needle and syringe. Pregnant macaques were monitored daily prior to and after viral inoculation for any clinical signs of infection (e.g., diarrhea, inappetence, inactivity, fever and atypical behaviors).

Inoculation and monitoring

Macaques were inoculated subcutaneously with $1x10^4$ PFU Zika virus/*H.sapiens-tc/PUR/2015/PRVABC59_v3c2* (PRVABC59, GenBank: KU501215). This virus was originally isolated from a traveler to Puerto Rico and passaged three times on Vero cells (American Type

Culture Collection (ATCC): CCL-81). The seed stock was obtained from Brandy Russell (CDC, Ft. Collins, CO). Virus stocks were prepared by inoculation onto a confluent monolayer of C6/36 cells (*Aedes albopictus* mosquito larval cells; ATCC: CCL-1660) with two rounds of amplification. The animals were anesthetized as described above, and 1 mL of inoculum at 1 x 10^4 PFU dilution in PBS was administered subcutaneously over the cranial dorsum. Post-inoculation, the animals were closely monitored by veterinary and animal care staff for adverse reactions or any signs of disease.

Pregnancy monitoring and fetal measurements

Weekly ultrasounds were conducted to observe the health of the fetus and to obtain measurements including fetal femur length (FL), biparietal diameter (BPD), head circumference (HC), and heart rate as previously described (60). Growth curves were developed for FL, BPD, and HC. Mean measurements and standard deviations at specified days of gestation in rhesus macaques were retrieved from Tarantal et al. (67) and the ultrasound measurements were plotted against this normative data. Doppler ultrasounds to measure fetal heart rate were performed biweekly.

vRNA isolation from body fluids and tissues

RNA was extracted from 300 µl of plasma using the Viral Total Nucleic Acid Purification kit (Promega, Madison, WI, USA) on a Maxwell 16 MDx instrument. qRT-PCR was performed as previously described (68). The limit of quantification for the assay is 100 copies/mL for qRT-PCR from plasma.

Fetal and maternal-fetal interface tissues were preserved with RNAlater® (Invitrogen, Carlsbad, CA) immediately following collection. RNA was isolated from maternal and fetal tissues using the Trizol Plus RNA Purification kit (Invitrogen, Carlsbad, CA) following the manufacturer's instructions or a similar method described by Hansen et al. (69). In the latter method, RNA was

recovered from up to 200 mg of tissue disrupted in TRIzol (Life Technologies, Waltham, MA) with 2 x 5 mm stainless steel beads using the TissueLyser (Qiagen, Hilden, Germany) for 3 minutes at 25 r/s twice. Following homogenization, samples in TRIzol were separated using Bromo-chloro-propane (Sigma). The aqueous phase was collected and glycogen was added as a carrier. The samples were washed in isopropanol and ethanol precipitated. RNA was fully re-suspended in 5 mM tris pH 8.0.

Plaque reduction neutralization test (PRNT)

Macaque serum samples were screened for ZIKV neutralizing antibodies using a plaque reduction neutralization test (PRNT). Endpoint titrations of reactive sera, using a 90% cutoff (PRNT90), were performed as described (70) against ZIKV strain PRVABC59. Briefly, ZIKV was mixed with serial 2-fold dilutions of serum for 1 hour at 37°C prior to being added to Vero cells and neutralization curves were generated using GraphPad Prism software (La Jolla, CA). The resulting data were analyzed by nonlinear regression to estimate the dilution of serum required to inhibit 90% of infection.

Whole virion ZIKV-specific binding antibody ELISA

High-binding 96-well ELISA plates (Greiner; Monroe, NC) were coated with 40 ng/well of 4G2 monoclonal antibody, which was produced in a mouse hybridoma cell line (D1-4G2-4-15, ATCC; Manassas, VA), diluted to 0.8 ng/uL in 0.1M carbonate buffer (pH 9.6) and incubated overnight at 4°C. Plates were blocked in 1X Tris-buffered saline containing 0.05% Tween-20 and 5% normal goat serum (cat.# G6767, Sigma-Aldrich, St. Louis, MO) or 1 hour at 37°C, followed by an incubation with 1.15 x 10^5 focus-forming units (ffu)/well Zika virus (PRVABC59, BEI; Manassas, VA) for 1 hour at 37°C. Plasma samples were tested at a dilution of 1:12.5-204,800 in serial 4-fold dilutions and incubated for 1 hour at 37°C, along with a ZIKV-specific monoclonal antibody, H24 (10 ug/mL), isolated from a ZIKV-infected rhesus macaque. Horseradish

peroxidase (HRP)-conjugated mouse anti-monkey IgG secondary antibody (Southern BioTech; Birmingham, AL) was used at a 1:4,000 dilution and incubated at 37°C for 1 hour, followed by the addition of SureBlue Reserve TMB Substrate (KPL; Gaithersburg, MD). Reactions were terminated by Stop Solution (KPL; Gaithersburg, MD) after a 7-minute incubation per plate in the dark. Optical density (OD) was detected at 450 nm on a Victor X Multilabel plate reader (PerkinElmer; Waltham, MA). Binding was considered detectable if the sample OD value at the lowest dilution was greater than that of the background OD, defined as the OD value of the negative control at the lowest dilution plus 2 standard deviations (SD). For samples considered positive, their OD values for the serial dilution were entered into Prism v8 (GraphPad Software; San Diego, CA) to determine the 50% effective dilution (ED_{50}). Briefly, the ED_{50} was calculated by transforming the fold dilution into log_{10}. The transformed data was then analyzed using a sigmoidal dose-response nonlinear regression model. Any sample considered negative was assigned an ED_{50} of 12.5, the lowest dilution tested, because ED_{50} cannot be accurately calculated below the lowest dilution tested.

The log_{10} 50% effective dilutions (ED_{50}) were calculated for IgG binding responses against the whole virion and compared between 0, 7, 14 and 28 dpi time points.

ZIKV IgM enzyme-linked immunosorbent assay (ELISA)

Infant macaque serum samples were screened for anti-ZIKV IgM antibodies using commercial human anti-ZIKV IgM ELISA assays targeting ZIKV nonstructural protein 1 (NS1) antigen. We utilized a sandwich ELISA (cat# ab213327, Abcam, Cambridge, Massachusetts, USA) and an indirect ELISA (cat# el26689601M, Euroimmun, Mountain Lakes, New Jersey, USA). Manufacturer instructions were followed. Positive and negative controls run in each assay included manufacturer-provided human serum samples and rhesus macaque serum collected at 0 and 14 days post-infection with PRVABC59 from an adult rhesus macaque (animal ID 244667). Infant serum samples were run in triplicate. All samples and controls were read on a

Synergy HTX plate reader at 450 nm. Sample values were reported in "Abcam units" (Abcam) or "ratio" (Euroimmun), which are the ratio of sample serum absorbance to the absorbance of a manufacturer-provided solution containing the upper limit of the reference range of non-infected biological sample ("cutoff" (Abcam) or "calibrator" (Euroimmun)). This method of reporting results is recommended by the manufacturers to control for inter-assay variability.

Cesarean delivery and maternal necropsy

ZIKV-exposed infants were delivered by Cesarean section at approximately 155 gestational days (gd), except for the single fetal demise at 133 gd. Amniotic fluid was collected prior to infant delivery via aspiration with a syringe and needle inserted through the membranes into the amniotic fluid. Sterile instruments were used for the dissection and collection of all maternal and maternal-fetal interface tissues during the gross post-mortem examination. Each tissue was collected with a unique set of sterile instruments and placed in a separate sterile petri dish before transfer to RNAlater for ZIKV qRT-PCR or fixed for histology, to prevent cross-contamination.

Infant care

After delivery, infants were dried, stimulated and received respiratory support as necessary, and placed in a warmed incubator. All liveborn ZIKV-exposed infants were transferred to the nursery where they remained until euthanasia and necropsy on day of life 7-8. ZIKV-exposed infants were reared in the nursery to enable continuous access to the infants for testing and to prevent confounding of maternal rearing differences on neurobehavior. During this period, multiple examinations were completed, including an eye exam, optical coherence tomography, visual electrophysiology studies, auditory brain response testing, brain MRI and three neurobehavioral assessments (Fig 10). Control infants for these assessments were obtained from the breeding colony or from other WNPRC research studies involving infants reared in the nursery (S1 table).

Neurobehavioral assessments

The Schneider Neonatal Assessment for Primates (SNAP) (19), a 20 minute battery of developmental tests, was administered at 1, 3-5, and 6-7 days of life (DOL), with the day of birth considered DOL 0 to four ZIKV-exposed infants (424847, 499874, 527421, 226691) and one age-matched control infant (020501) (S1 table) . This assessment, similar to the human Brazelton Newborn Behavioral Assessment Scale (21) captures detailed developmental behaviors in macaques less than 1 month of age. The SNAP assesses neonatal neurobehavior using 68 individually scored test items (S11 table) in four subscales (motor maturity and activity, orientation, sensory, and state control). Testing occurred midway between feedings at approximately the same time each day. Ratings were based on a five point Likert scale ranging from 0 to 2. Examiners were trained in standardized administration and scoring procedures by the SNAP developer, M. Schneider, requiring a check-out protocol prior to administration. Two examiners were present for all neurobehavioral testing and scoring to ensure test administration reliability (>95%). Graphs were prepared in RStudio (2015, Integrated Development for R. RStudio, Inc., Boston, MA).

Feeding volume and weight gain analysis

Cumulative feeding volume from DOL 0 to DOL 8 was evaluated by measuring the formula feeding volume infants took at each feeding from their medical record. For the two control infants that were placed in the nursery on DOL 1 because of maternal rejection, their feeding volume was measured beginning on DOL 1. For analyses, the cumulative feeding volumes of these two control infants (r18052 and r18076) were started at 0 ml rather than making assumptions or estimations about their feeding volumes prior to placement in the nursery on DOL 1. Cumulative feeding volumes over time were compared between ZIKV-exposed and control groups using a linear mixed effects model with animal specific random effects. A

compound symmetry correlation structure was used to analyze weight and cumulative feeding volume and conduct comparisons between cohorts, and gestational age at birth was included as a covariate in these analyses given the differences between the ZIKV-exposed and control infants' gestational ages at birth. To determine whether there was evidence for an outlier in the ZIKV-exposed infant group cumulative feeding volume trajectories, a chi-square outlier test was performed and confirmed using alternative outlier tests (Dixon and Grubbs outlier tests). All reported P-values are two-sided and $p<0.05$ was used to define statistical significance. Statistical analyses were conducted using SAS software (SAS Institute Inc., Cary NC), version 9.4) and R (the R Foundation for Statistical Computing) version 3.5.1.

Brain MRI

Data acquisition

Neuroimaging data were collected on 4 ZIKV-exposed infants at 7 days of age and on 13 age-matched controls infants using a 3T MRI scanner (GE750, GE Healthcare, Waukesha, WI) with a Tx/Rx 8-channel volume coil. Data were acquired in a single session that included T1 scan with the parameters: repetition time (TR) = 9272 ms, echo time (TE) = 4064 ms, $\theta = 12°$, field of view (FOV) = 100 × 100 mm, slice thickness = 0.8 mm. Animals were scanned in the supine position in the same orientation, achieved by placement and immobilization of the head in a custom-made head holder via ear bars. Scans were collected under anesthesia described in S12 table. End-tidal CO_2, inhaled CO_2, O_2 saturation, heart rate, respiratory rate, blood pressure and body temperature were monitored continuously and maintained during each MRI session.

Data processing

Data were analyzed using the module of DPARSF v4.4 for the subsection of Monkey Data, which is part of the Data Processing and Analysis of Brain Imaging (DPABI) toolbox v3.1 (http://rfmri.org/dpabi) (38, 71). DPABI is a plug-in software based on Statistical Parametric

Mapping (SPM v12) and Resting-State fMRI Data Analysis Toolkit plus (RESTplus, v1.2) integrated in Matlab2017 (71). The Digital Imaging and Communications in Medicine (DICOM) files were first arranged and the parameters (such as time points, TR, slice number, voxel size etc.) were then set. DPARSF then produced the preprocessed data (with slice timing, realignment, normalization, and smoothing). The first five volumes were discarded to allow the magnetization to approach a dynamic equilibrium.

Data processing was performed as previously described for human data processing (38), except for spatial normalization (resampling voxel size of 2 × 2 × 2 mm). A spatial Gaussian filter of 3 mm FWHM (full-width at half maximum) was used for smoothing. The individual monkey T1 structural image is coregistered to the functional image. Then, using the monkey prior tissue probability maps generated by McLaren et al. (72), the transformed structural image is segmented into grey matter (GM), white matter (WM) and cerebrospinal fluid (CSF) through unified segmentation (73). The structural volumes are normalized to the 112RM-SL space using the normalization parameters estimated during unified segmentation (72, 74) The remaining steps follow the human processing pipeline (38).

Group differences of the grey matter volume and density between ZIKV and control groups were examined using the independent two-sample t-test in the module of Statistical Analysis in DPABI. Sex and postnatal age were covariates. The group differences were visualized with the Viewer (with 112RM-SL_T1 template) in DPABI.

Ophthalmic exam

Infants were anesthetized as described in S12 table for eye exams. Pupillary reactivity was assessed and intraocular pressures were obtained prior to eye dilation with ophthalmic drops

(0.05% proparacaine, tropicamide, phenylephrine). Slit-lamp biomicroscopy and indirect ophthalmoscopy were performed after pupillary dilation.

Optical coherence tomography

Spectral-domain optical coherence tomography (SD-OCT) scans of the retina and anterior segment were carried out in both eyes of most infants using a Heidelberg™ Spectralis HRA + OCT (Heidelberg™ Engineering, Heidelberg, Germany) instrument. Quantitative evaluation of scans included total retinal thickness, as well as thickness of the retinal nerve fiber layer, ganglion cell layer, inner plexiform layer, inner nuclear layer, outer plexiform layer, outer nuclear layer, photoreceptor inner segment, photoreceptor outer segment, choroid and central cornea. Segmentation and determination of corneal and retinal layer thickness was performed using combined manual and automatic segmentation algorithms from both Heidelberg and EXCELSIOR (75). EXCELSIOR Preclinical's functionalities for retinal segmentation (EdgeSelect™) and automated image analysis were used to calculate mean thicknesses for retinal layers. Multivariate analysis of variance (MANOV) with animal specific random effects was used to compare layer thickness between ZIKV-exposed and control infant groups. Corrected gestational age was included as a covariate to adjust the comparisons by corrected gestational age. Least squared adjusted means and the corresponding 95% confidence intervals are reported. All reported P-values are two-sided and $p<0.05$ was used to define statistical significance. All analyses were conducted using SAS software (SAS Institute Inc., Cary NC), version 9.4. Graphs were prepared in RStudio (2015, Integrated Development for R. RStudio, Inc., Boston, MA).

Visual electrophysiology

Photopic full-field ERGs (ffERG) to a series of flash strengths and photopic flash visual-evoked potentials (fVEP), were recorded, in that order. Measurements were recorded under anesthesia

using a BigShot™ electrodiagnostic system (LKC Technologies™, Gaithersburg, MD). If isoflurane was used during an early procedure in the same sedation event, a washout period was allowed before visual electrophysiology studies to minimize isoflurane suppression of cortical activity (76). Corneas were anesthetized with topical 0.5% proparacaine prior to application of ERG-149 jet™ (Universo™, Switzerland) contact lens electrodes and a conductive wetting solution. Reference electrodes were subdermal stainless-steel needle electrodes inserted near the ipsilateral outer canthus of each eye. Visual evoked potentials were recorded from two active subdermal electrodes situated approximately 1 cm superior to the occipital ridge and 1 cm lateral to the midline; VEP reference electrodes were situated adjacent to one another along the midline at the vertex. Replicates (2-4) of 80 flashes each were performed on each macaque. ERG and VEP waveforms were processed off-line and machine scored using software written in Matlab™ (Nattick, MA). fVEPs were quantified as the root-mean-square of the response from 50-150 msec post flash. Amplitude and latency measurements and root-mean-square measurements were analyzed using a linear mixed effects analysis with animal specific random effects and comparisons were adjusted by corrected gestational age (covariate). A compound symmetry correlation was used to account for correlations between multiple outcome measures. Side (right vs. left), cohort (ZIKV vs. control) and the interaction between side and cohort were included as predictor variables in the model using SAS version 9.4 (SAS Institute Inc., Cary, NC). Least squares adjusted means and the corresponding 95% confidence intervals were reported. Graphs were prepared in RStudio (2015, Integrated Development for R. RStudio, Inc., Boston, MA).

Auditory brain response testing

Hearing was evaluated by measuring auditory brain responses, a neurologic test of auditory brainstem function in response to auditory stimuli. In this evaluation, an evoked potential is generated by an auditory stimuli transmitted from an earphone and the elicited waveform

response is measured by subdermal electrodes (77). Auditory brain response (ABR) thresholds were obtained for auditory (click) stimuli using the Biologic Navigator Pro system. Ambient noise levels was minimized. For the ABR, needle electrodes were placed at the brow ridge (positive input) and behind the right pinna (negative input) for channel 1 and from the brow ridge (positive input) and behind the left pinna (negative input) for channel 2. An electrode was placed below the brow ridge on the forehead for the ground. Electrode impedances were below 10 kohm for all electrodes. Physiological filters were set to pass 100–3000 Hz. The stimuli were clicks with rarefaction and condensation alternating polarity and a Blackman window with 2-ms rise-fall and 1 ms plateau times. Insert earphones (Etymotic ER-3A) were used to obtain the click thresholds. Signal levels were presented at 70, 50, and 30 dB nHL. Wave V was observed at each presentation level.

Infant or fetus necropsy

Infants delivered from ZIKV-infected dams were sedated and euthanized on day of life 7 or 8, as described in Figure 10. Fetus 416597 was stillborn and was submitted to necropsy immediately after delivery. Sterile instruments were used for the dissection and collection of all tissues during gross post-mortem examinations. Each tissue was collected with a unique set of sterile instruments and placed in a separate sterile petri dish before transfer RNAlater for ZIKV qRT-PCR or 4% paraformaldehyde for histology. Ten slices of the fetal/infant cerebrum (~5 mm in thickness) were prepared in the coronal plane with section 1 located most anteriorly and section 10 located most posteriorly, and three slices of the cerebellum were prepared in the sagittal plane with section 1 located most laterally and section 3 most medially; alternate sections were taken for qRT-PCR to analyze vRNA and for histology.

Histology

Tissues were fixed in 4% PFA other than cerebrum, cerebellum and one eye for histology which were fixed in 10% neutral buffered formalin. All tissues were sectioned (~5 mm), routinely processed and embedded in paraffin. Paraffin sections (5 µm) were stained with hematoxylin and eosin (HE) or Gram stain using standard methods. The pathologists were blinded to vRNA findings when evaluating and describing tissue sections and assigning morphologic diagnoses. Photomicrographs were obtained using brightfield microscopes Olympus BX43 and Olympus BX46 (Olympus Inc., Center Valley, PA) with attached Olympus DP72 digital camera (Olympus Inc.) and Spot Flex 152 64 Mp camera (Spot Imaging, Sterling Heights, MI), and captured using commercially available image-analysis software (cellSens DimensionR, Olympus Inc. and Spot 5.3 Software). The ear diagram used to describe where ear sections were obtained from is a composite of multiple histologic sections of infant 020501 with the addition of an external pinna based on gross images.

In situ hybridization

In situ hybridization (ISH) was conducted either in brain tissues post-fixed in neutral buffered formalin or in non-brain tissues post-fixed in 4% PFA for 24 hours, and alcohol processed and paraffin embedded. ISH probes against Zika genome were purchased commercially (Advanced Cell Diagnostics, Cat No. 468361, Newark, California, USA). ISH was performed using the RNAscope® Red 2.5 Kit (Advanced Cell Diagnostics, Cat No. 322350) according to the manufacturer's instructions. Briefly, after deparaffinization with xylene, a series of ethanol washes, and peroxidase blocking, sections were heated in antigen retrieval buffer and then digested by proteinase. Sections were exposed to ISH target probe and incubated at 40°C in a hybridization oven for 2 h. After rinsing, ISH signal was amplified using company-provided Pre-amplifier followed by the Amplifier containing labelled probe binding sites and developed with a Fast Red chromogenic substrate for 10 min at room temperature. Sections were then stained with hematoxylin, air-dried, and mounted. Positive control probes for endogenous rhesus

macaque mRNA (Advanced Cell Diagnostics, Cat No. 457711, Newark, California, USA) and negative control probes for bacterial mRNA (Advanced Cell Diagnostics, Cat No. 310043, Newark, California, USA) were used as process controls to verify ISH labelling procedure was successful. Mouse brain tissue served as a positive control for ZIKV ISH in brain tissues and mouse spleen served as a positive control for ZIKV ISH in non-brain tissues.

Data availability

Primary data that support the findings of this study are available at the Zika Open-Research Portal (https://zika.labkey.com/project/OConnor/Manuscripts/Pharyngeal%20motor%20cortex%20grey%20matter%20abnormalities%20and%20retinal%20photoreceptor%20layer%20dysfunction%20in%20macaques%20exposed%20to%20Zika%20virus%20in%20utero/begin.view?). Zika virus/H.sapiens-tc/PUR/2015/PRVABC59-v3c2 sequence data have been deposited in the Sequence Read Archive (SRA) with accession code SRX2975259. All other data supporting the findings of this study are available within the article and its supplementary information files.

Acknowledgements

We thank Nathan Diers, Seth Eaton and Peter Cueno for assistance with OCT segmentation. We thank Clara R. Landucci for making the ear illustration.

Figure legends

Figure 1. Pregnancy experimental design, maternal plasma vRNA loads and maternal antibody responses. (A) Pregnant macaques were inoculated with ZIKV-PR in the first trimester and one female had a stillbirth at 133 gestational days (gd). Maternal blood was

obtained at the times indicated for each animal (vertical lines on each animal's timeline) and ultrasound analyses of the fetus and placenta were performed weekly (black vertical lines). (B) Maternal plasma vRNA loads were measured by qRT-PCR. (C) Estimated EC90 values for serum neutralization of ZIKV assessed prior to infection, 7 dpi, 28 dpi and at maternal necropsy. (D) Estimated EC50 values for serum ZIKV IgG titers obtained prior to infection, 7 dpi, 28 dpi and at maternal necropsy. The dashed line indicates the limit of detection.

Figure 2. Fetal head growth during pregnancy. Fetal ultrasonography depicting head circumference (A) and biparietal diameter (B) during gestation. The growth curve standard deviation (SD) was calculated from normative fetal rhesus macaque measurements (67).

Figure 3. Decidua, placental bed and placental villous pathology. (A-F) Chronic lymphoplasmacytic deciduitis (asterisks) is present in 3 of 5 ZIKV-exposed placentas (C, D, E) and the control decidua (F), and not in 2 of 5 ZIKV-exposed placentas (A, B). There is perivascular lymphocytic infiltration in (B) with no plasma cells, a normal finding. (G-L) Uterine placental bed histology reveals minimal to severe lymphoplasmacytic myometritis or suppurative to lymphoplasmacytic endometritis (caret symbol) in 4 of 5 ZIKV-exposed dams (G, H, I, K) and not in one of the ZIKV-exposed dams (J) or control decidua (L). (M-R) Within the placenta, 3 of the 5 ZIKV-exposed pregnancies have villitis (arrow heads) (N, O, P) and not in 2 of the ZIKV-exposed dams (M, Q) or a control placental villi ((R). Colors of macaques in each image represent individual animals as depicted at the top of the figure. Scale bar is 100 μm.

Figure 4. Viral loads and ISH in the maternal-fetal interface. (A) Viral loads were assessed in female reproductive and fetal extraembryonic tissues by qRT-PCR at delivery and sections of some of these tissues were assessed by ISH. (B) Positive ZIKV ISH in the decidua of dam

664184. (C) Positive ISH staining in the amniotic/chorionic membrane of fetus 416597. NT = not tested, NC = not collected, NA = not applicable.

Figure 5. Infant weight gain and cumulative feeding volume. (A) Color key for individual infants along with combined trendlines for the control group of infants (black) or ZIKV-exposed infants (brown). (B) Cumulative feeding volumes and (C) weights were measured while the infants were in the nursery. Dashed lines indicate the values of individual infants and solid lines indicate the trend line for each group.

Figure 6. Neurobehavioral assessment. (A) Animal IDs of the ZIKV-exposed and control neonates. The (B) Motor Maturity and Activity construct, (C) Orientation construct, (D) Sensory construct and (E) State Control construct were assessed on three separate days (Trials 1-3) during the infants' 8 days of life before necropsy, as described in S1 table. Test items are scored from 0-2, with 0 representing no response or performance and 0 2 representing a higher performance of the measured behaviors.

Figure 7. Retinal and choroidal layer thicknesses measured by optical coherence tomography. (A) Retinal layer segmentation was performed using EXCELSIOR Preclinical, and layers are marked as an example from infant 424847. (B) Thicknesses of the retina, central cornea and choroid were measured in the ZIKV-exposed and control infants with the designated color scheme. Values from the left and right eyes are demonstrated with a circle and a square, respectively. (C) Retinal layer thicknesses were measured using the segmentation demonstrated in part A for ZIKV exposed and control infants. Both the right and left eyes were measured in all animals except for animal 499874 whose left eye was not able to be measured due to anesthesia limitations. Linear mixed effects analysis adjusted for corrected gestational

age comparing the ZIKV-exposed and control infants: *p = 0.0012, ^p = 0.0179, #p = 0.0011, +p = 0.0102.

Figure 8. Electroretinography and visual evoked potentials. (A) ZIKV-exposed and control infants underwent visual electrophysiology studies. Right and left eye values were graphed separately with a square or circle, respectively. (B) Light-adapted ERGs were performed for each infant and the amplitude and latency of the A and B waves were recorded (as described in S7 figure). (C) Visual evoked potentials were performed on an uncovered right or left eye, and the amplitude, latency (as described in S7 figure) and room-mean-square of the N2 and P2 waves were recorded. *p-value = 0.042 for the left eye A wave latency when comparing the left eye A wave latencies.between the ZIKV-exposed and control infant groups.

Figure 9. MRI analysis and voxel-based morphometry comparison.

(A) Voxel-based morphometry analysis of 4 ZIKV-exposed infants and 13 age-matched controls identifies increased grey matter volume and density of 4 ZIKV-exposed infants compared with controls. The red highlighted regions indicate the specific locations where the ZIKV-exposed infant group had higher grey matter volume and density than control infants. L: left; R: right; A: anterior; P: posterior. The color scale represents the fold-increase of the grey matter volume and density above the controls. (B) t-values and specific stereotaxic locations grey matter volume and density differences between ZIKV-exposed and control infants. Sex and age were considered as covariates. (C) Coronal Bravo T1 images of each ZIKV-exposed infant through the precentral gyrus, where the differences in grey matter were identified using voxel-based morphometry. The region where the grey matter changes were identified are marked with a white rectangle.

Figure 10. ZIKV-exposed infant examination schedule. Infants were evaluated by neurobehavioral assessment (NBAS), ophthalmic exam (OP), optical coherence tomography (OCT), auditory brain response (ABR), visual electrophysiology (EP) and brain MRI prior to euthanasia and necropsy (NX). Urine (*) and blood (#) were collected at the indicated times.

Figure 11. Fetus/Infant tissue histopathology of the ear. Neutrophilic otitis media (40x inset) is present in 3 of 5 ZIKV-exposed fetus/infants (A, C, D) and not in a control infant (F) or two ZIKV-exposed infants (B, E). (G) Ear diagram depicting where tissue sections were obtained for the 2x and 40x magnifications. Macaque colors represent animals as depicted at the top of the figure. Arrowheads denote the location of the neutrophilic inflammation. Scale bar is 100 μm.

Figure 12. Fetus/Infant tissue histopathology of the lymph node and lung.
(A-F) Neutrophilic lymphadenitis is present in 3 of 5 ZIKV-exposed infants (B, C, E) and in a control infant lymph node (F), but not in 2 of the ZIKV-exposed infants (A, D) (images with neutrophilic lymphadenitis are denoted with an asterisk). (G-L) Diffuse bronchopneumonia is present in 2 of 5 ZIKV-exposed infants (I, K) but not in a control infant (L) or 3 of the ZIKV-exposed infants (G, H, J) (images with bronchopneumonia are denoted with an asterisk). The lung in the stillborn macaque (G) is atelectatic (uninflated) due to stillbirth. Macaque colors represent individual animals as depicted at the top of the figure. Scale bar is 100 μm.

References

1. Rice ME, Galang RR, Roth NM, Ellington SR, Moore CA, Valencia-Prado M, et al. Vital Signs: Zika-Associated Birth Defects and Neurodevelopmental Abnormalities Possibly

Associated with Congenital Zika Virus Infection - U.S. Territories and Freely Associated States, 2018. MMWR Morbidity and mortality weekly report. 2018;67(31):858-67.

2. Hoen B, Schaub B, Funk AL, Ardillon V, Boullard M, Cabie A, et al. Pregnancy Outcomes after ZIKV Infection in French Territories in the Americas. The New England journal of medicine. 2018;378(11):985-94.

3. Calle-Giraldo JP, Rojas CA, Hurtado IC, Barco C, Libreros D, Sanchez PJ, et al. Outcomes of Congenital Zika Virus Infection During an Outbreak in Valle del Cauca, Colombia. The Pediatric infectious disease journal. 2019.

4. Rodo C, Suy A, Sulleiro E, Soriano-Arandes A, Maiz N, Garcia-Ruiz I, et al. Pregnancy outcomes after maternal Zika virus infection in a non-endemic region: prospective cohort study. Clinical microbiology and infection : the official publication of the European Society of Clinical Microbiology and Infectious Diseases. 2019.

5. Brady OJ, Osgood-Zimmerman A, Kassebaum NJ, Ray SE, de Araujo VEM, da Nobrega AA, et al. The association between Zika virus infection and microcephaly in Brazil 2015-2017: An observational analysis of over 4 million births. PLoS medicine. 2019;16(3):e1002755.

6. Adebanjo T, Godfred-Cato S, Viens L, Fischer M, Staples JE, Kuhnert-Tallman W, et al. Update: Interim Guidance for the Diagnosis, Evaluation, and Management of Infants with Possible Congenital Zika Virus Infection - United States, October 2017. MMWR Morbidity and mortality weekly report. 2017;66(41):1089-99.

7. Wheeler AC, Ventura CV, Ridenour T, Toth D, Nobrega LL, Silva de Souza Dantas LC, et al. Skills attained by infants with congenital Zika syndrome: Pilot data from Brazil. PloS one. 2018;13(7):e0201495.

8. Melo A, Gama GL, Da Silva Junior RA, De Assuncao PL, Tavares JS, Da Silva MB, et al. Motor function in children with congenital Zika syndrome. Developmental medicine and child neurology. 2019.

9. Nielsen-Saines K, Brasil P, Kerin T, Vasconcelos Z, Gabaglia CR, Damasceno L, et al. Delayed childhood neurodevelopment and neurosensory alterations in the second year of life in a prospective cohort of ZIKV-exposed children. Nature medicine. 2019.

10. Vianna RAO, Lovero KL, Oliveira SA, Fernandes AR, Santos T, Lima L, et al. Children Born to Mothers with Rash During Zika Virus Epidemic in Brazil: First 18 Months of Life. Journal of tropical pediatrics. 2019.

11. Mohr EL. Modeling Zika Virus-Associated Birth Defects in Nonhuman Primates. Journal of the Pediatric Infectious Diseases Society. 2018;7(suppl_2):S60-s6.

12. Osuna CE, Whitney JB. Nonhuman Primate Models of Zika Virus Infection, Immunity, and Therapeutic Development. The Journal of infectious diseases. 2017;216(suppl_10):S928-s34.

13. Dudley DM, Aliota MT, Mohr EL, Newman CM, Golos TG, Friedrich TC, et al. Using Macaques to Address Critical Questions in Zika Virus Research. Annual review of virology. 2019.

14. Mavigner M, Raper J, Kovacs-Balint Z, Gumber S, O'Neal JT, Bhaumik SK, et al. Postnatal Zika virus infection is associated with persistent abnormalities in brain structure, function, and behavior in infant macaques. Science translational medicine. 2018;10(435).

15. Ultrasound screening for fetal microcephaly following Zika virus exposure. American journal of obstetrics and gynecology. 2016;214(6):B2-4.

16. Leal MC, van der Linden V, Bezerra TP, de Valois L, Borges ACG, Antunes MMC, et al. Characteristics of Dysphagia in Infants with Microcephaly Caused by Congenital Zika Virus Infection, Brazil, 2015. Emerging infectious diseases. 2017;23(8):1253-9.

17. van der Linden V, Pessoa A, Dobyns W, Barkovich AJ, Junior HV, Filho EL, et al. Description of 13 Infants Born During October 2015-January 2016 With Congenital Zika Virus Infection Without Microcephaly at Birth - Brazil. MMWR Morbidity and mortality weekly report. 2016;65(47):1343-8.

18. Alves LV, Paredes CE, Silva GC, Mello JG, Alves JG. Neurodevelopment of 24 children born in Brazil with congenital Zika syndrome in 2015: a case series study. BMJ open. 2018;8(7):e021304.

19. Schneider ML, Suomi SJ. Neurobehavioral Assessment in Rhesus Monkey Neonates (Macaca mulatta): Developmental Changes, Behavioral Stability and Early Experience. Infant Behavior and Development. 1992;15:155-77.

20. Coe CL, Lubach GR, Crispen HR, Shirtcliff EA, Schneider ML. Challenges to maternal wellbeing during pregnancy impact temperament, attention, and neuromotor responses in the infant rhesus monkey. Developmental psychobiology. 2010;52(7):625-37.

21. Brazelton TB. Assessment of the infant at risk. Clinical obstetrics and gynecology. 1973;16(1):361-75.

22. Laughlin NK, Lasky RE, Giles NL, Luck ML. Lead effects on neurobehavioral development in the neonatal rhesus monkey (Macaca mulatta). Neurotoxicology and teratology. 1999;21(6):627-38.

23. Schneider ML, Moore CF, Kraemer GW, Roberts AD, DeJesus OT. The impact of prenatal stress, fetal alcohol exposure, or both on development: perspectives from a primate model. Psychoneuroendocrinology. 2002;27(1-2):285-98.

24. Schneider ML, Roughton EC, Koehler AJ, Lubach GR. Growth and development following prenatal stress exposure in primates: an examination of ontogenetic vulnerability. Child development. 1999;70(2):263-74.

25. Yepez JB, Murati FA, Pettito M, Penaranda CF, de Yepez J, Maestre G, et al. Ophthalmic Manifestations of Congenital Zika Syndrome in Colombia and Venezuela. JAMA ophthalmology. 2017;135(5):440-5.

26. Bito LZ, Merritt SQ, DeRousseau CJ. Intraocular pressure of rhesus monkey (Macaca mulatta). I. An initial survey of two free-breeding colonies. Investigative ophthalmology & visual science. 1979;18(8):785-93.

27. Townes-Anderson E, Raviola G. Morphology and permeability of blood vessels in the prenatal rhesus monkey eye: how plasma components diffuse into the intraocular fluids during development. Experimental eye research. 1982;35(3):203-30.

28. Johnson PT. Clinical appearance of the hyaloid artery system in the newborn rhesus monkey. Journal of medical primatology. 1979;8(3):184-6.

29. Vinekar A, Mangalesh S, Jayadev C, Maldonado RS, Bauer N, Toth CA. Retinal Imaging of Infants on Spectral Domain Optical Coherence Tomography. Biomed Res Int. 2015;2015:782420-.

30. Robson AG, Nilsson J, Li S, Jalali S, Fulton AB, Tormene AP, et al. ISCEV guide to visual electrodiagnostic procedures. Documenta ophthalmologica Advances in ophthalmology. 2018;136(1):1-26.

31. Wong CW, Ng SR, Cheung CM, Wong TY, Mathur R. ZIKA-RELATED MACULOPATHY. Retinal cases & brief reports. 2017.

32. de Carvalho Leal M, Ramos DS, Caldas Neto SS. Hearing Loss From Congenital Zika Virus Infection. Topics in magnetic resonance imaging : TMRI. 2019;28(1):19-22.

33. Raymond LA, Wallace D, Berman NE, Marcario J, Foresman L, Joag SV, et al. Auditory brainstem responses in a Rhesus Macaque model of neuro-AIDS. Journal of neurovirology. 1998;4(5):512-20.

34. Kraus N, Smith DI, Reed NL, Willott J, Erwin J. Auditory brainstem and middle latency responses in non-human primates. Hearing research. 1985;17(3):219-26.

35. Brasil P, Pereira JP, Jr., Moreira ME, Ribeiro Nogueira RM, Damasceno L, Wakimoto M, et al. Zika Virus Infection in Pregnant Women in Rio de Janeiro. The New England journal of medicine. 2016;375(24):2321-34.

36. Kurth FL, E.; Gaser, C. Voxel-Based Morphometry. In: Toga AWB, P.; Thompson, P.; Friston, K., editor. Brain Mapping: An Encyclopedic Reference 1: Academic Press; 2015. p. 345-9.

37. Riva D, Bulgheroni S, Aquino D, Di Salle F, Savoiardo M, Erbetta A. Basal forebrain involvement in low-functioning autistic children: a voxel-based morphometry study. AJNR American journal of neuroradiology. 2011;32(8):1430-5.

38. Yan CG, Wang XD, Zuo XN, Zang YF. DPABI: Data Processing & Analysis for (Resting-State) Brain Imaging. Neuroinformatics. 2016;14(3):339-51.

39. Seeley WW, Crawford RK, Zhou J, Miller BL, Greicius MD. Neurodegenerative diseases target large-scale human brain networks. Neuron. 2009;62(1):42-52.

40. Brent BK, Thermenos HW, Keshavan MS, Seidman LJ. Gray matter alterations in schizophrenia high-risk youth and early-onset schizophrenia: a review of structural MRI findings. Child and adolescent psychiatric clinics of North America. 2013;22(4):689-714.

41. Bakhshi K, Chance SA. The neuropathology of schizophrenia: A selective review of past studies and emerging themes in brain structure and cytoarchitecture. Neuroscience. 2015;303:82-102.

42. Scott JA, Grayson D, Fletcher E, Lee A, Bauman MD, Schumann CM, et al. Longitudinal analysis of the developing rhesus monkey brain using magnetic resonance imaging: birth to adulthood. Brain structure & function. 2016;221(5):2847-71.

43. Mohr EL, Block LN, Newman CM, Stewart LM, Koenig M, Semler M, et al. Ocular and uteroplacental pathology in a macaque pregnancy with congenital Zika virus infection. PloS one. 2018;13(1):e0190617.

44. Lefton-Greif MA. Pediatric dysphagia. Physical medicine and rehabilitation clinics of North America. 2008;19(4):837-51, ix.

45. Michou E, Hamdy S. Cortical input in control of swallowing. Current opinion in otolaryngology & head and neck surgery. 2009;17(3):166-71.

46. Moore CA, Staples JE, Dobyns WB, Pessoa A, Ventura CV, Fonseca EB, et al. Characterizing the Pattern of Anomalies in Congenital Zika Syndrome for Pediatric Clinicians. JAMA pediatrics. 2016.

47. Greimel E, Nehrkorn B, Schulte-Ruther M, Fink GR, Nickl-Jockschat T, Herpertz-Dahlmann B, et al. Changes in grey matter development in autism spectrum disorder. Brain structure & function. 2013;218(4):929-42.

48. Wang J, Fu K, Chen L, Duan X, Guo X, Chen H, et al. Increased Gray Matter Volume and Resting-State Functional Connectivity in Somatosensory Cortex and their Relationship with Autistic Symptoms in Young Boys with Autism Spectrum Disorder. Frontiers in physiology. 2017;8:588.

49. Hsin YL, Harnod T, Chang CS, Peng SJ. Increase in gray matter volume and white matter fractional anisotropy in the motor pathways of patients with secondarily generalized neocortical seizures. Epilepsy research. 2017;137:61-8.

50. Groeschel S, Vollmer B, King MD, Connelly A. Developmental changes in cerebral grey and white matter volume from infancy to adulthood. International journal of developmental neuroscience : the official journal of the International Society for Developmental Neuroscience. 2010;28(6):481-9.

51. Chimelli L, Melo ASO, Avvad-Portari E, Wiley CA, Camacho AHS, Lopes VS, et al. The spectrum of neuropathological changes associated with congenital Zika virus infection. Acta neuropathologica. 2017;133(6):983-99.

52. Moreira ME. Vertical Exposure to Zika Virus and Its Consequences for Child Neurodevelopment (ZIKVIRUSIFF) [updated 5.3.18. Available from: https://ClinicalTrials.gov/show/NCT03255369.

53. Rojas MA. Neurodevelopment Outcome of Newborns Exposed to Zika Virus (ZIKV) in Utero 2019 [updated 1.17.19. Available from: https://ClinicalTrials.gov/show/NCT02943304.

54. Institut National de la Santé Et de la Recherche Médicale F. Zika Virus Infection's Neonatal and Pediatric Consequences in French Department of America [updated 8.30.16. Available from: https://ClinicalTrials.gov/show/NCT02810210.

55. Linsenmeier RA, Zhang HF. Retinal oxygen: from animals to humans. Progress in retinal and eye research. 2017;58:115-51.

56. Hirsch AJ, Roberts VHJ, Grigsby PL, Haese N, Schabel MC, Wang X, et al. Zika virus infection in pregnant rhesus macaques causes placental dysfunction and immunopathology. Nature communications. 2018;9(1):263.

57. Aleman TS, Ventura CV, Cavalcanti MM, Serrano LW, Traband A, Nti AA, et al. Quantitative Assessment of Microstructural Changes of the Retina in Infants With Congenital Zika Syndrome. JAMA ophthalmology. 2017;135(10):1069-76.

58. Zhao Z, Yang M, Azar SR, Soong L, Weaver SC, Sun J, et al. Viral Retinopathy in Experimental Models of Zika Infection. Investigative ophthalmology & visual science. 2017;58(10):4355-65.

59. Waldorf KMA, Nelson BR, Stencel-Baerenwald JE, Studholme C, Kapur RP, Armistead B, et al. Congenital Zika virus infection as a silent pathology with loss of neurogenic output in the fetal brain. Nature medicine. 2018.

60. Nguyen SM, Antony KM, Dudley DM, Kohn S, Simmons HA, Wolfe B, et al. Highly efficient maternal-fetal Zika virus transmission in pregnant rhesus macaques. PLoS pathogens. 2017;13(5):e1006378.

61. Martinot AJ, Abbink P, Afacan O, Prohl AK, Bronson R, Hecht JL, et al. Fetal Neuropathology in Zika Virus-Infected Pregnant Female Rhesus Monkeys. Cell. 2018.

62. Syggelou A, Fanos V, Iacovidou N. Acute otitis media in neonatal life: a review. Journal of chemotherapy (Florence, Italy). 2011;23(3):123-6.

63. Bergus GR, Levy BT, Levy SM, Slager SL, Kiritsy MC. Antibiotic use during the first 200 days of life. Archives of family medicine. 1996;5(9):523-6.

64. de Fatima Viana Vasco Aragao M, van der Linden V, Petribu NC, Valenca MM, Parizel PM, de Mello RJV. Congenital Zika Syndrome: The Main Cause of Death and Correspondence

Between Brain CT and Postmortem Histological Section Findings From the Same Individuals. Topics in magnetic resonance imaging : TMRI. 2019;28(1):29-33.

65. Zwaigenbaum L, Bauman ML, Choueiri R, Fein D, Kasari C, Pierce K, et al. Early Identification and Interventions for Autism Spectrum Disorder: Executive Summary. Pediatrics. 2015;136 Suppl 1:S1-9.

66. Hennessey M, Fischer M, Staples JE. Zika Virus Spreads to New Areas - Region of the Americas, May 2015-January 2016. MMWR Morbidity and mortality weekly report. 2016;65(3):55-8.

67. Tarantal AF. Ultrasound Imaging in Rhesus (Macaca mulatta) and Long-tailed (Macaca fascicularis) Macaques: Reproductive and Research Applications. Ultrasound Imaging: Elsevier Ltd.; 2005.

68. Dudley DM, Aliota MT, Mohr EL, Weiler AM, Lehrer-Brey G, Weisgrau KL, et al. A rhesus macaque model of Asian-lineage Zika virus infection. Nature communications. 2016;7:12204.

69. Hansen SG, Piatak M, Jr., Ventura AB, Hughes CM, Gilbride RM, Ford JC, et al. Immune clearance of highly pathogenic SIV infection. Nature. 2013;502(7469):100-4.

70. Lindsey HS, Calisher CH, Mathews JH. Serum dilution neutralization test for California group virus identification and serology. Journal of clinical microbiology. 1976;4(6):503-10.

71. Chao-Gan Y, Yu-Feng Z. DPARSF: A MATLAB Toolbox for "Pipeline" Data Analysis of Resting-State fMRI. Frontiers in systems neuroscience. 2010;4:13-.

72. McLaren DG, Kosmatka KJ, Oakes TR, Kroenke CD, Kohama SG, Matochik JA, et al. A population-average MRI-based atlas collection of the rhesus macaque. NeuroImage. 2009;45(1):52-9.

73. Ashburner J, Friston KJ. Unified segmentation. NeuroImage. 2005;26(3):839-51.

74. McLaren DG, Kosmatka KJ, Kastman EK, Bendlin BB, Johnson SC. Rhesus macaque brain morphometry: a methodological comparison of voxel-wise approaches. Methods (San Diego, Calif). 2010;50(3):157-65.

75. Huang Y, Danis RP, Pak JW, Luo S, White J, Zhang X, et al. Development of a semi-automatic segmentation method for retinal OCT images tested in patients with diabetic macular edema. PloS one. 2013;8(12):e82922.

76. Sitdikova G, Zakharov A, Janackova S, Gerasimova E, Lebedeva J, Inacio AR, et al. Isoflurane suppresses early cortical activity. Annals of clinical and translational neurology. 2014;1(1):15-26.

77. Hall III JW. New Handbook of Auditory Evoked Responses: Pearson; 2006. 736 p.

Supplementary Figure legends

S1 figure. PRNT and and whole virion ELISA dose response curves.

S2 figure. Fetal abdominal circumference, femur length and heart rate measurements.

S3 figure. Representative images of fetal ultrasound abnormalities.

S4 figure. Infant IgM titers, body fluid viral loads and PRNTs. Sera from ZIKV-exposed infants were evaluated for the presence of ZIKV-specific IgM by two commercial assays: Abcam (A) and Euroimmun (B). The manufacturer provided positive and negative human IgM controls are shown in grey. Pre and post-ZIKV infection serum collected from an adult rhesus macaque (244667) was used as a species-specific positive and negative control (shown in black). The

dashed line indicates the positive cutoff value for each assay. (C) Infant body fluids (plasma, urine, CSF) were assessed for the presence of ZIKV RNA by qRT-PCR at the days indicated and were negative. NA, not applicable (because no samples were available from the stillborn fetus). (D) PRNTs were performed on infant serum from DOL 2-5 from liveborn infants and ED90 values were reported in comparison with maternal PRNT ED90 values from necropsy.

S5 figure. Infant PRNT dose response curves.

S6 figure. Hearing testing (auditory brain response testing) in ZIKV-exposed and control infants. Wave V latencies from auditory brain response (ABR) testing in a ZIKV-exposed infant (226691) and two control infants (r17104, 020501).

S7 figure. Scoring of representative ERG and VEP waveforms. These ERG and VEP waveforms were recorded simultaneously from control infant r18076. Red solid arrows: amplitude of labelled waveform features. ERG A- and VEP N2-wave amplitudes are measured relative to pre-flash voltage; ERG B-and VEP P2-wave amplitude measured from preceding A- and N2-waves, respectively (horizontal dotted line). Red dashed arrows: latency-to-peak, all measured from the onset of the flash stimulus (vertical dotted line). The neonatal rhesus photopic ERG contains a prominent short-latency wave (*) prior to the B-wave that decreases in prominence with age and was not quantified for this study.

S8 figure. RNAscope assay for the localization of ZIKV RNA by ISH in brain tissues from ZIKV-exposed infants. (A) ZIKV genomic RNA (red dots) in a ZIKV-exposed murine lateral geniculate brain section (20x). ZIKV-exposed fetus/infant brain sections exposed to ZIKV RNA probe (10x) (B) 527421 cerebral cortex (rostral to LGN), (C) 499874 cerebral cortex, (D) 226691

cerebral cortex, (E) 424847 cerebrum containing the lateral geniculate nucleus, (F) 416597 cerebellar brain section.

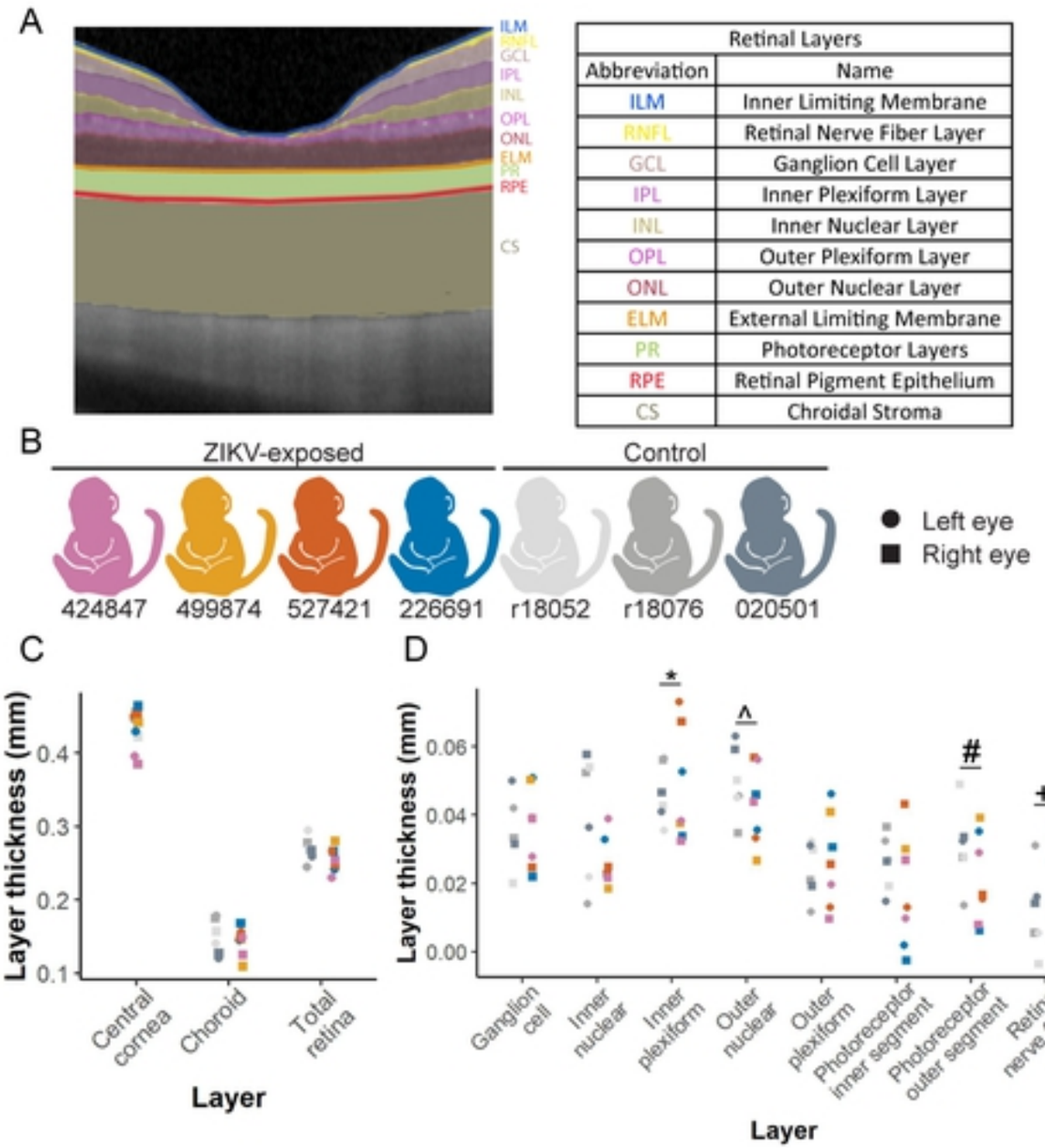

Retinal Layers	
Abbreviation	Name
ILM	Inner Limiting Membrane
RNFL	Retinal Nerve Fiber Layer
GCL	Ganglion Cell Layer
IPL	Inner Plexiform Layer
INL	Inner Nuclear Layer
OPL	Outer Plexiform Layer
ONL	Outer Nuclear Layer
ELM	External Limiting Membrane
PR	Photoreceptor Layers
RPE	Retinal Pigment Epithelium
CS	Chroidal Stroma

Figure 7

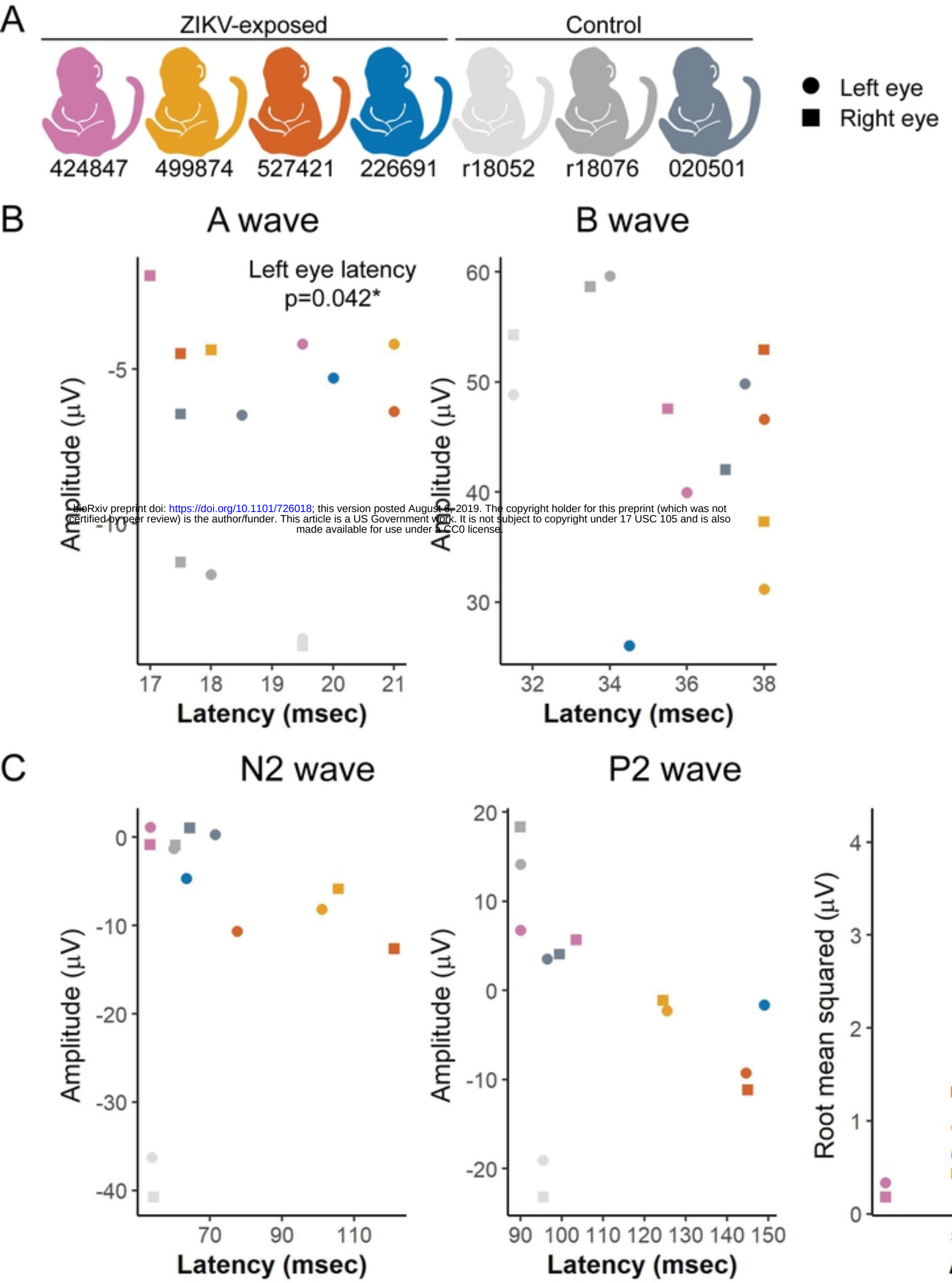

Figure 8

A

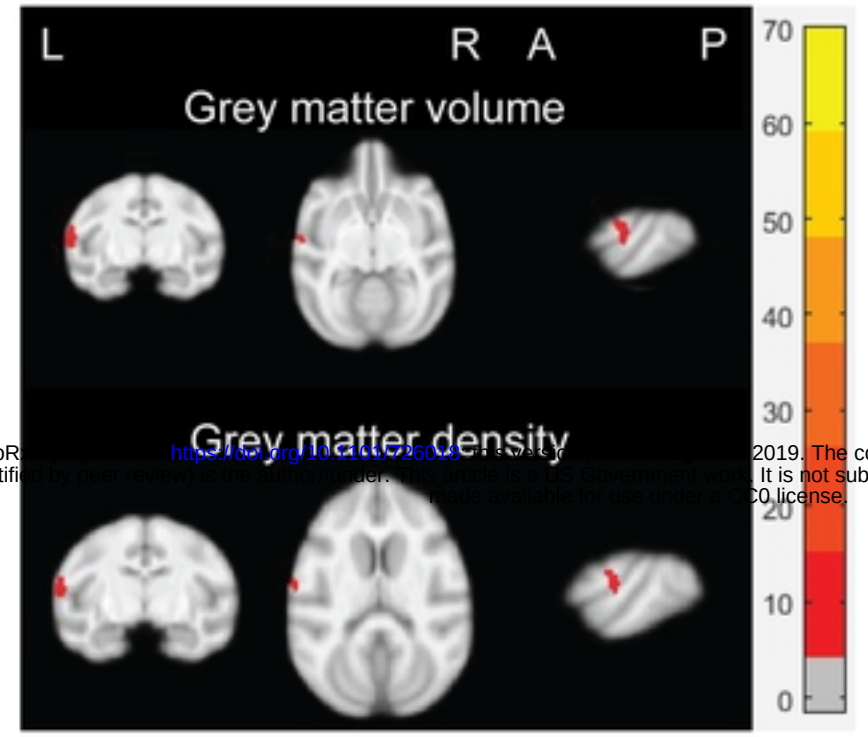

B

Regions	Stereotaxic coordinates			*t-value*
	x	*y*	*z*	
Gray matter volume				
Left precentral gyrus	-27	14	14	5.162
Left superior frontal gyrus	-27	14	19	4.925
Gray matter density				
Left precentral gyrus	-26	14	15	5.143
Left superior frontal gyrus	-26	15	20	4.611

C

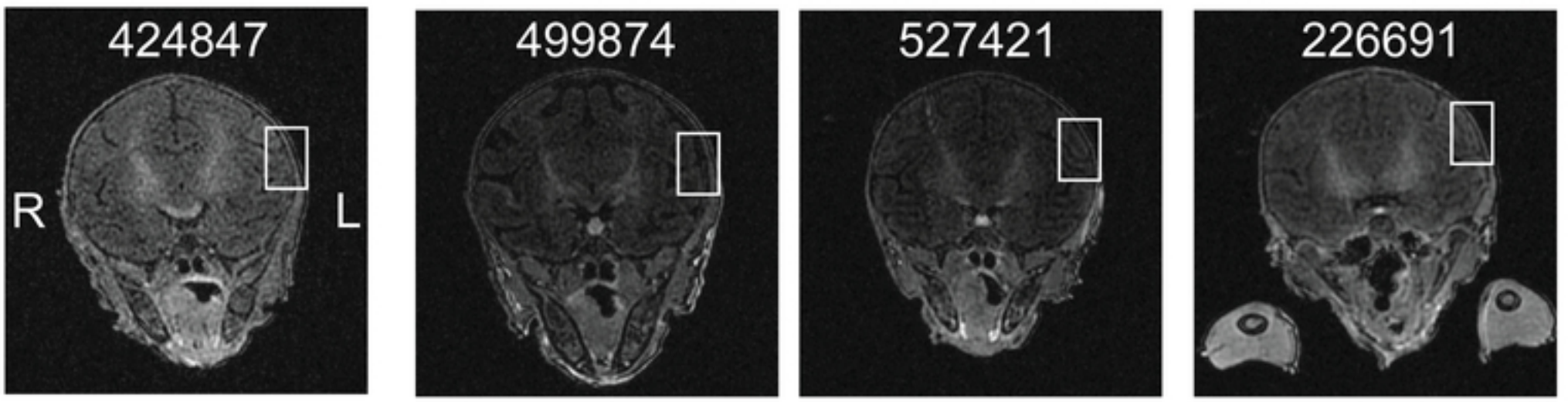

Figure 9

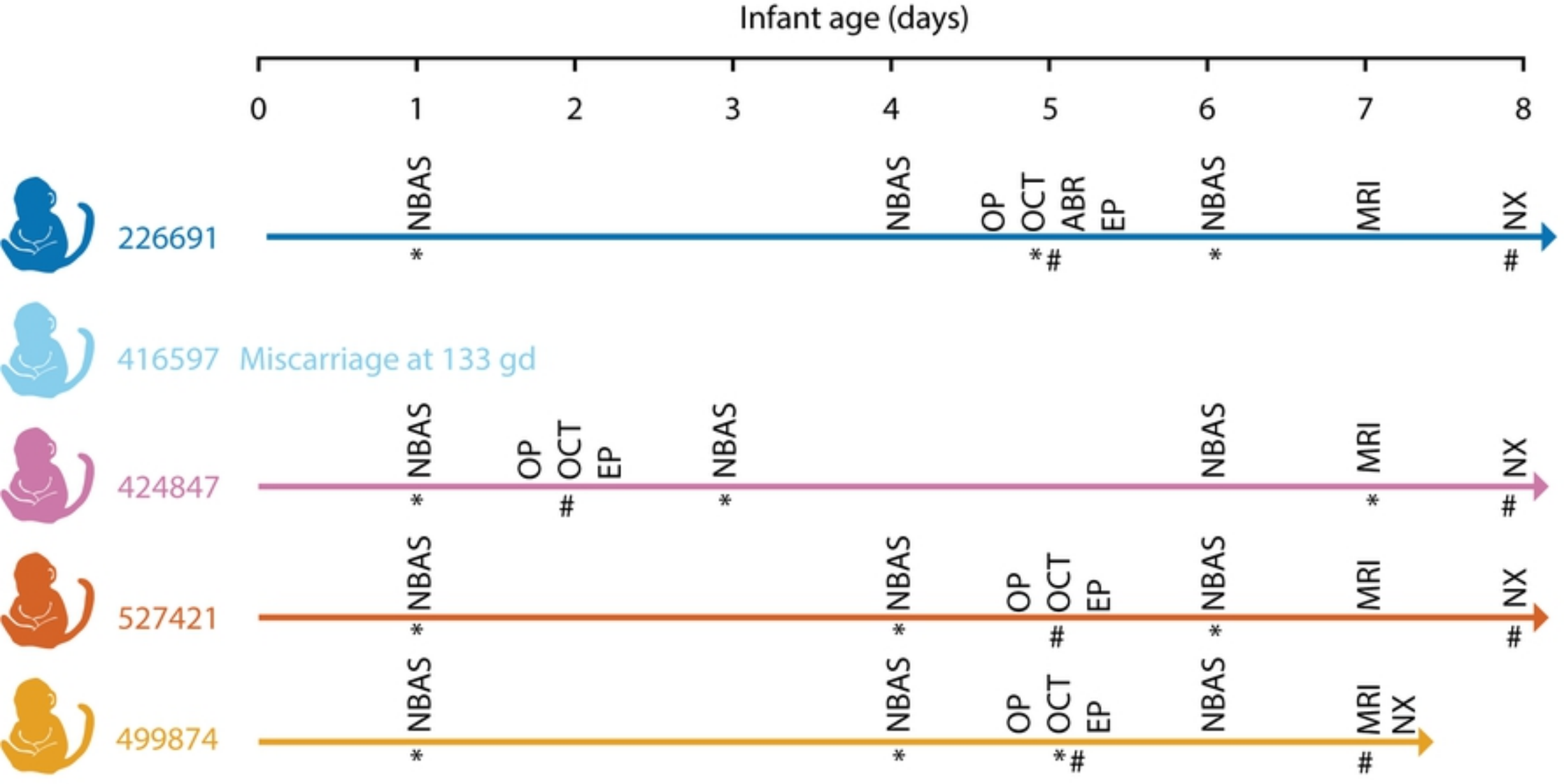
Infant age (days)
0
1
2
3
4
5
6
7
8
226691
NBAS
NBAS
OP
OCT
ABR
EP
NBAS
MRI
NX
416597 Miscarriage at 133 gd
424847
NBAS
OP
OCT
EP
NBAS
NBAS
MRI
NX
527421
NBAS
NBAS
OP
OCT
EP
NBAS
MRI
NX
499874
NBAS
NBAS
OP
OCT
EP
NBAS
MRI
NX

Figure 10

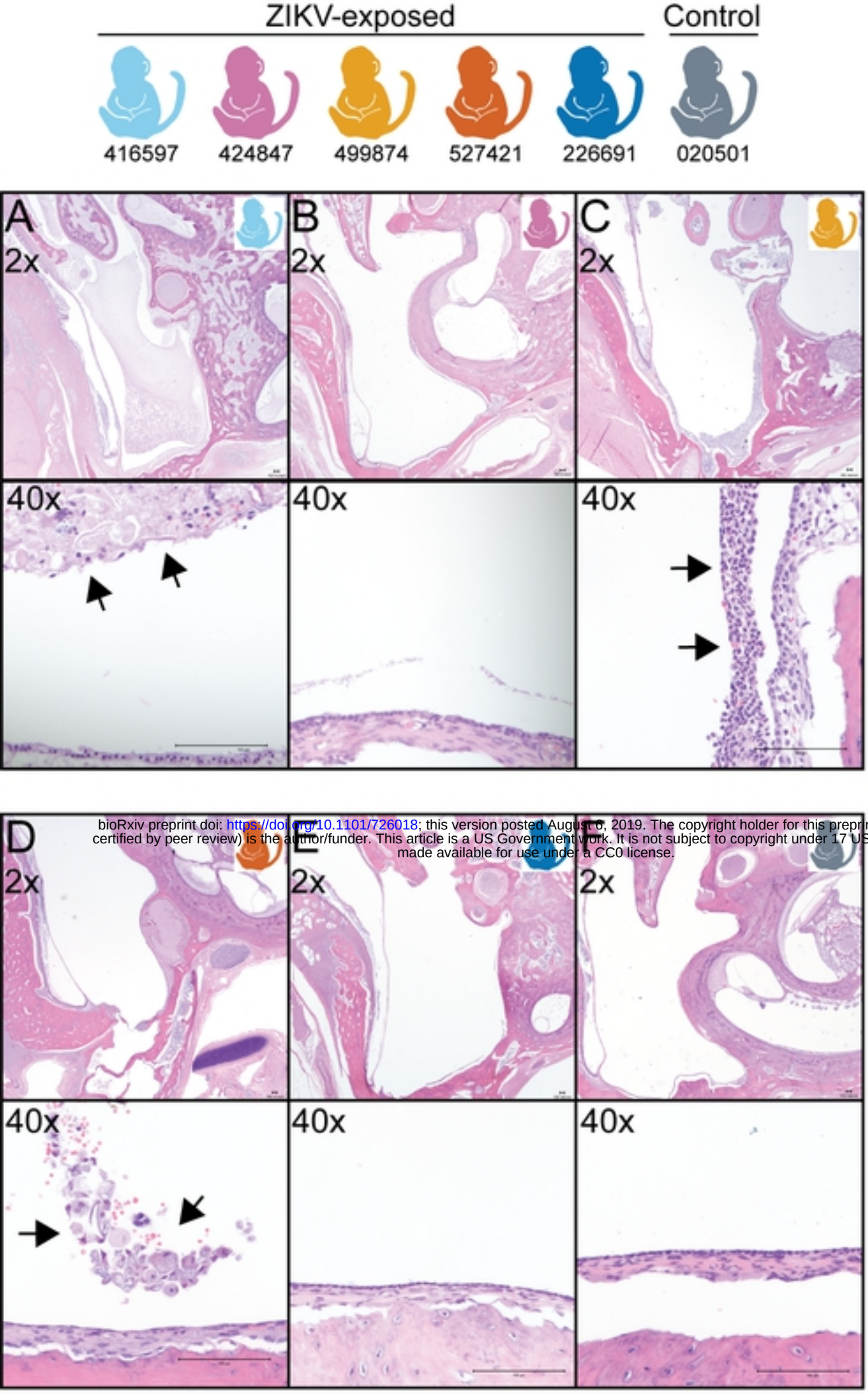

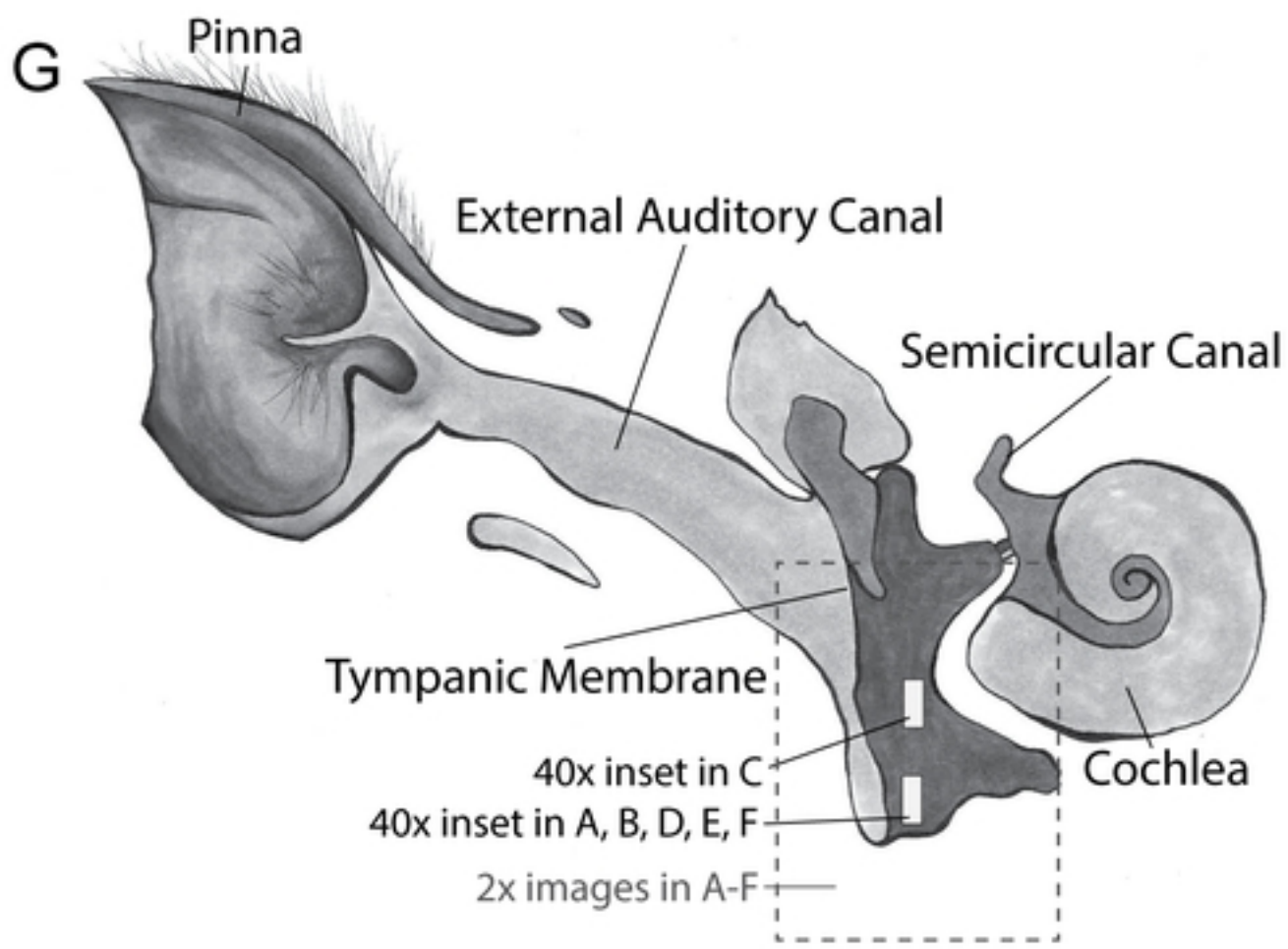

Figure 11

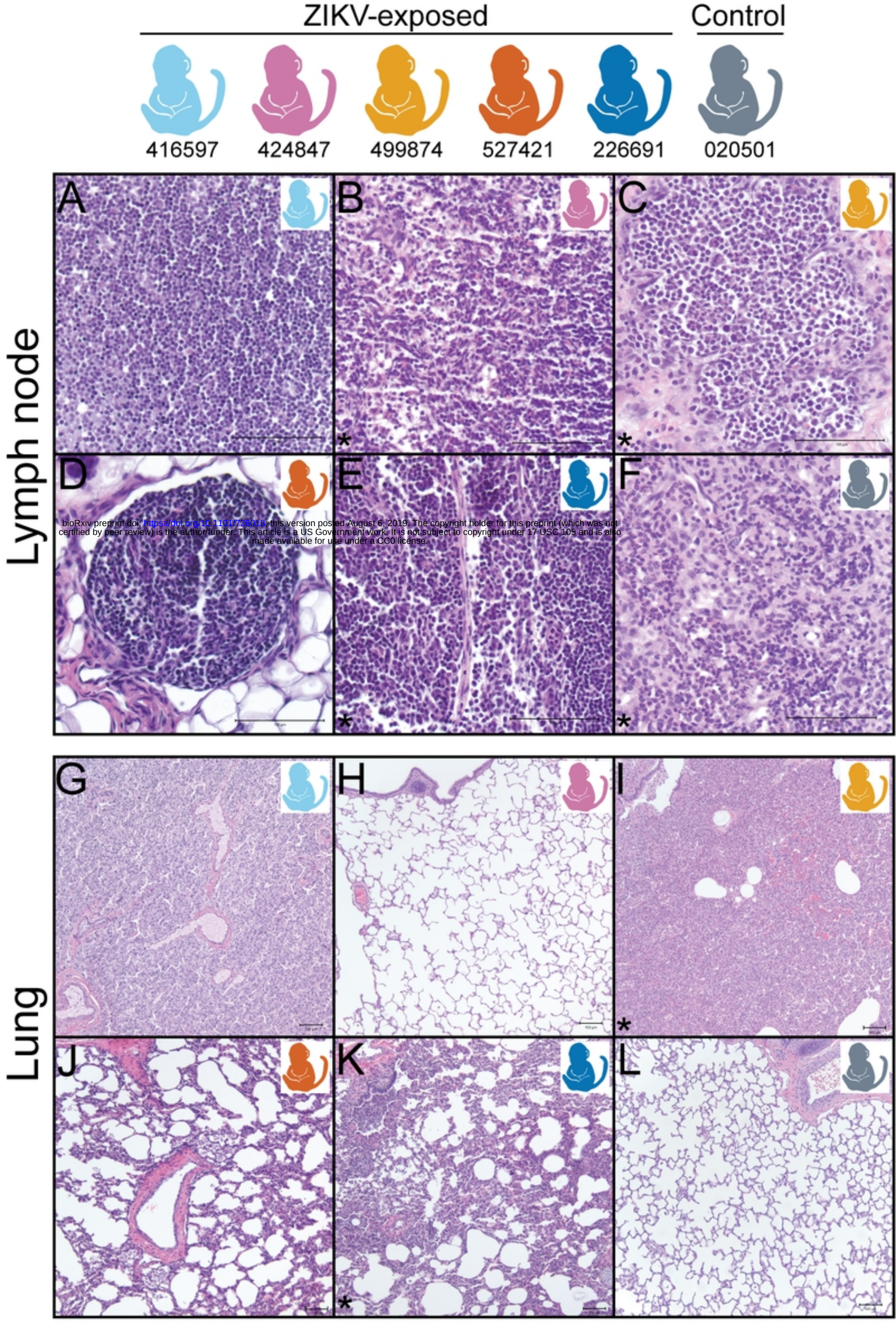

Figure 12

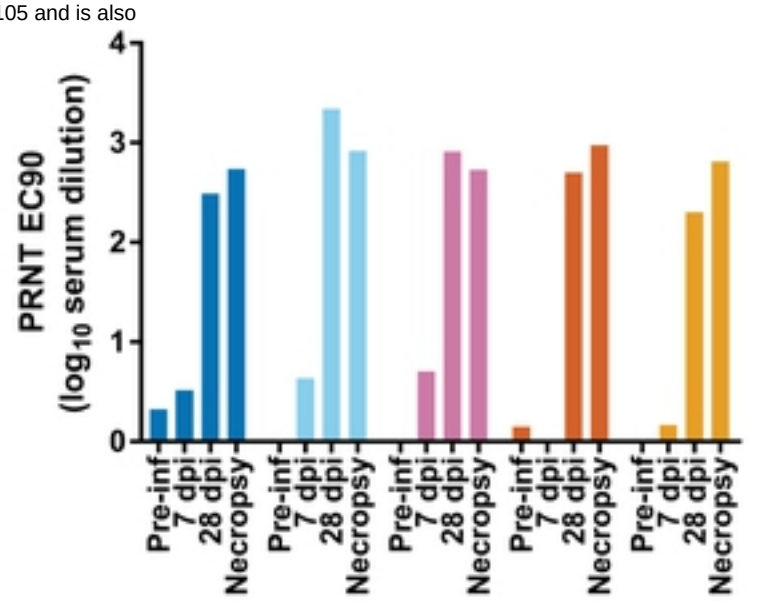

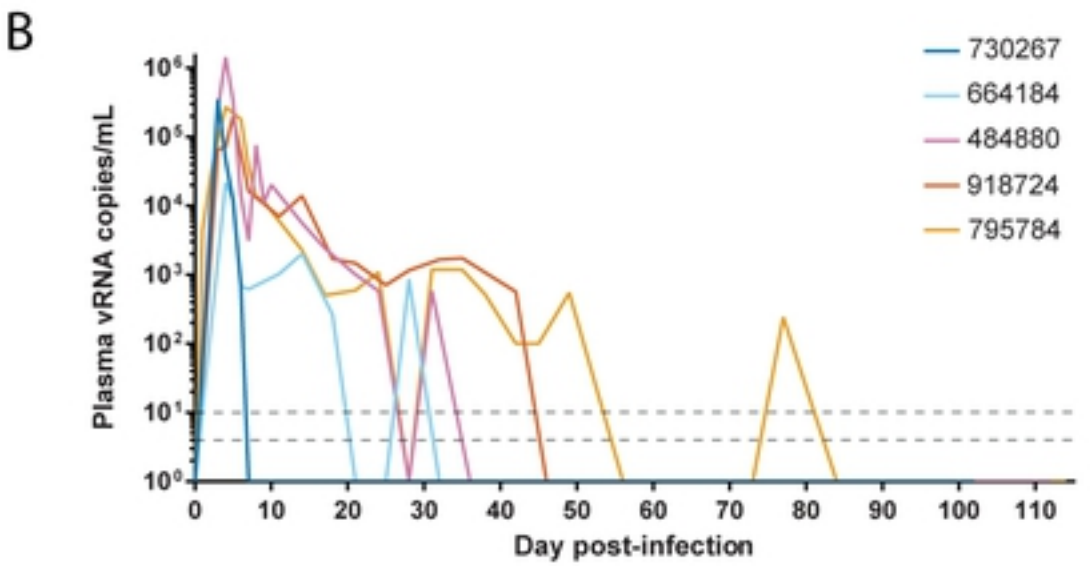

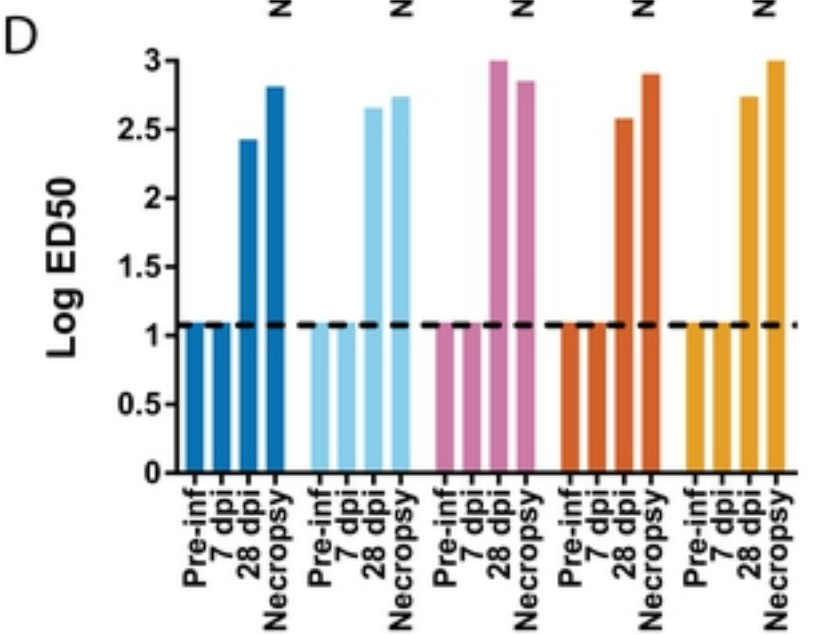

Figure 1

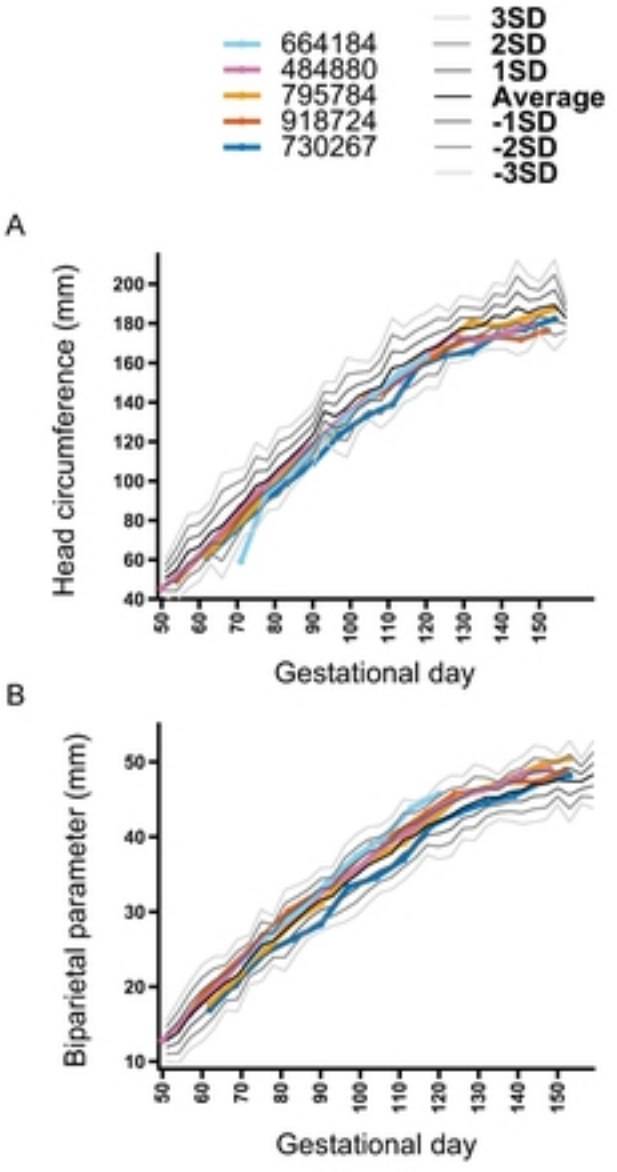
664184
484880
795784
918724
730267
3SD
2SD
1SD
Average
-1SD
-2SD
-3SD
A
Head circumference (mm)
Gestational day
B
Biparietal parameter (mm)
Gestational day

Figure 2

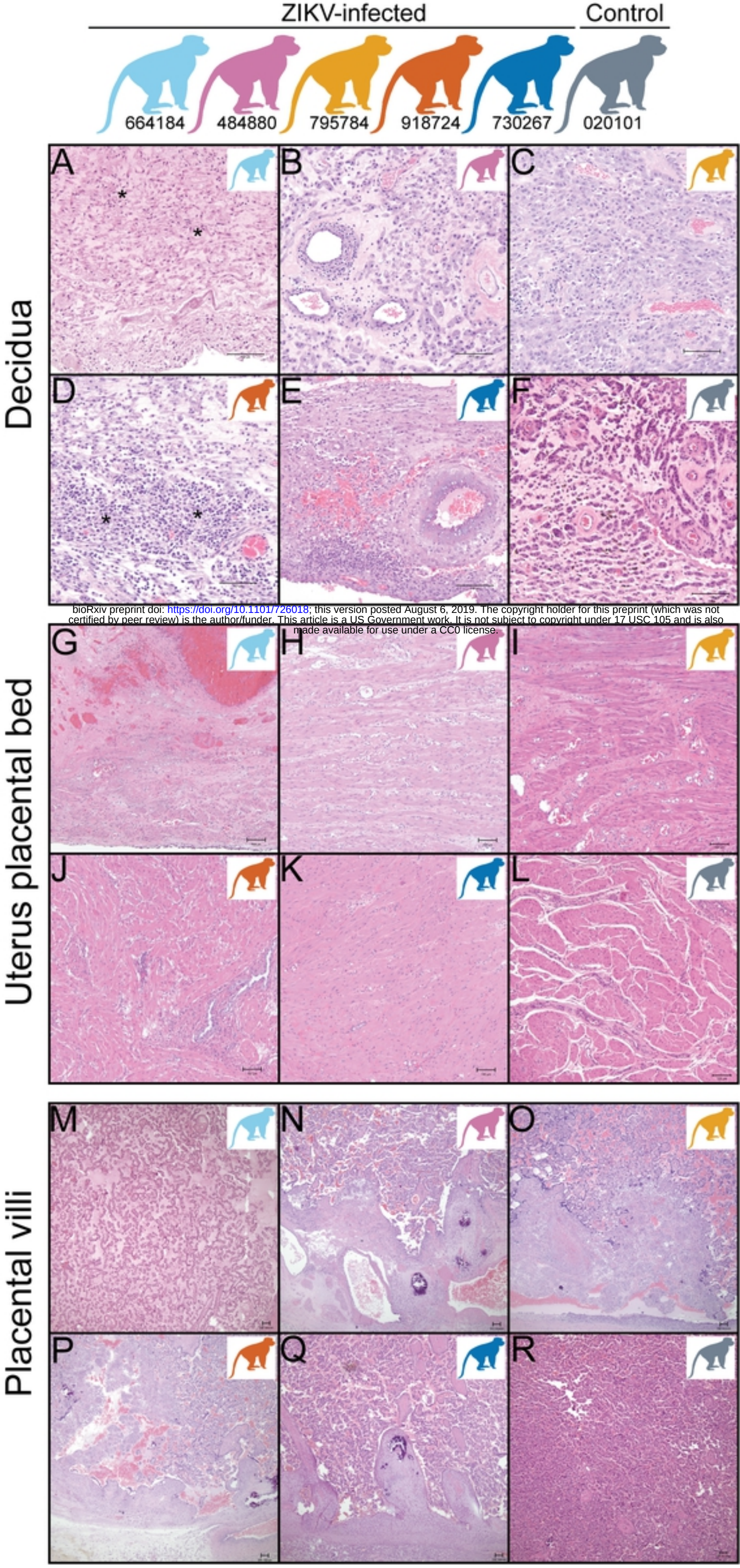

Figure 3

A

Tissue Source	Tissue Name	Animal ID (dam ID/fetus-infant ID)									
		664184/416597		484880/424847		795784/499874		918724/527421		730267/226691	
		qRT-PCR	ISH	qRT-PCR	ISH	qRT-PCR	ISH	qRT-PCR	ISH	qRT-PCR	ISH
Maternal tissues	Decidua	0	positive	0	negative	56 copies vRNA/mg	negative	0	negative	0	negative
	Placental bed	0	NT	0	NT	0	NT	0	NT	0	NT
	Uterus	0	NT	0	NT	0	NT	0	NT	0	NT
	Vagina	0	NT	0	NT	0	NT	0	NT	0	NT
Fetal extraembryonic tissues	Amniotic/chorionic membrane	0	positive	0	negative	0	negative	0	negative	0	negative
	Placental disc 1	0	negative	0	negative	0	negative	0	negative	0	negative
	Placental disc 2	0	negative	0	negative	0	negative	0	negative	0	negative
	Umbilical cord	0	NT	0	NT	0	NT	0	NT	0	NT
	Amniotic fluid	NC	NA	0	NA	0	NA	0	NA	0	NA

B

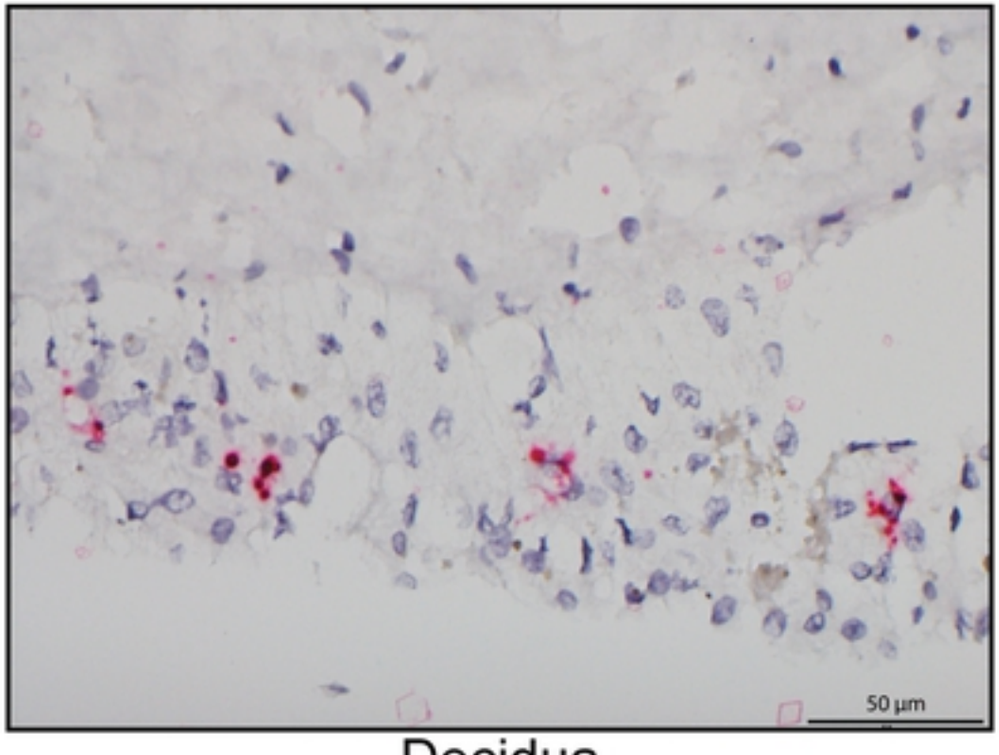

Decidua

C

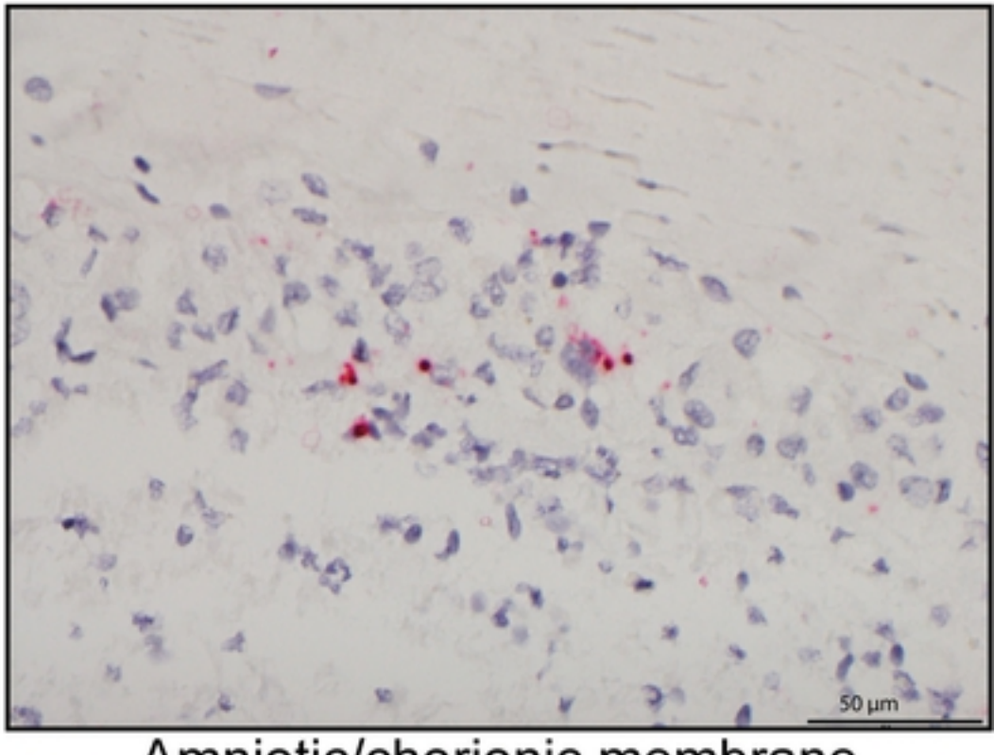

Amniotic/chorionic membrane

Figure 4

A

B

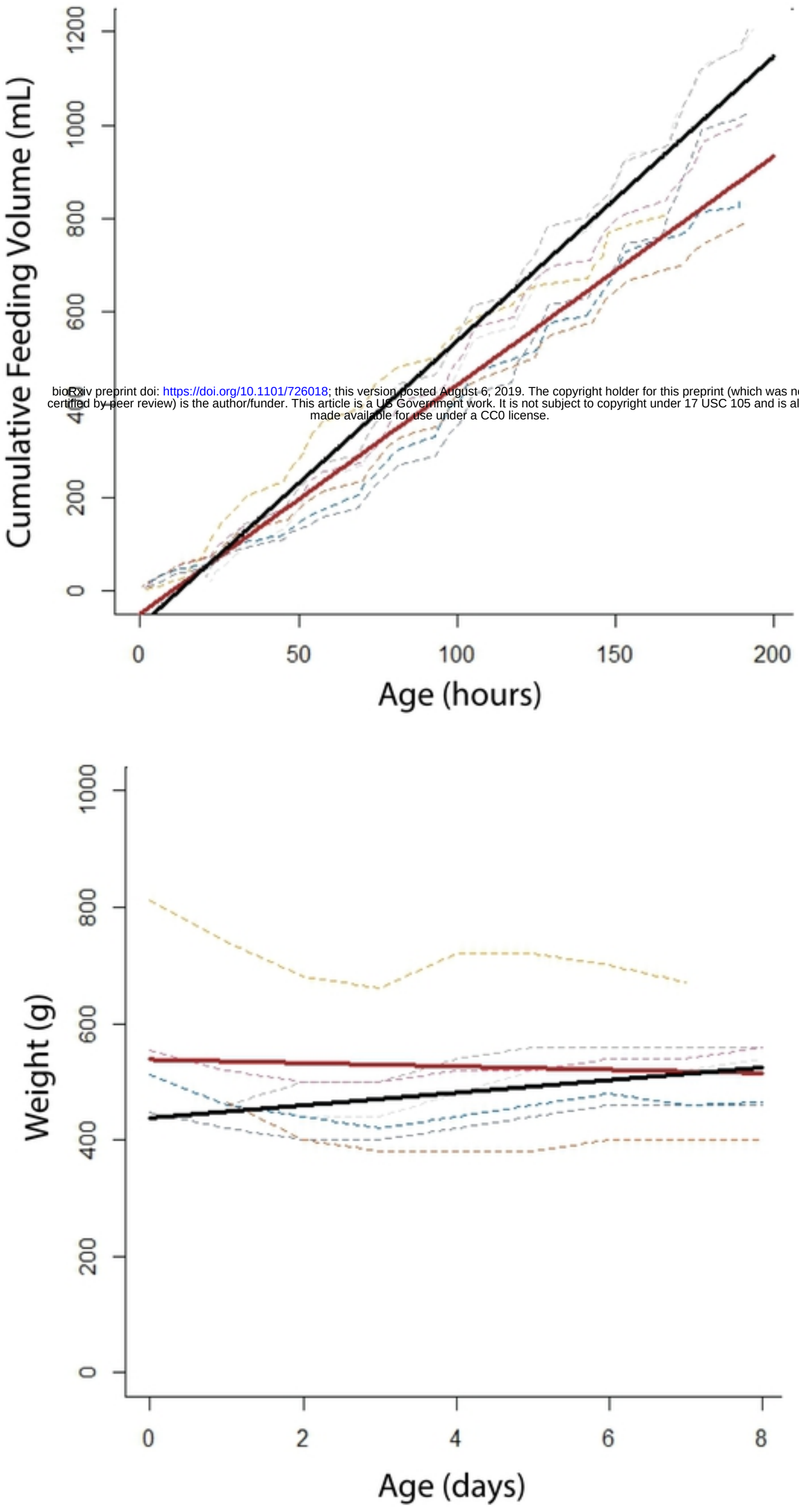

C

Figure 5

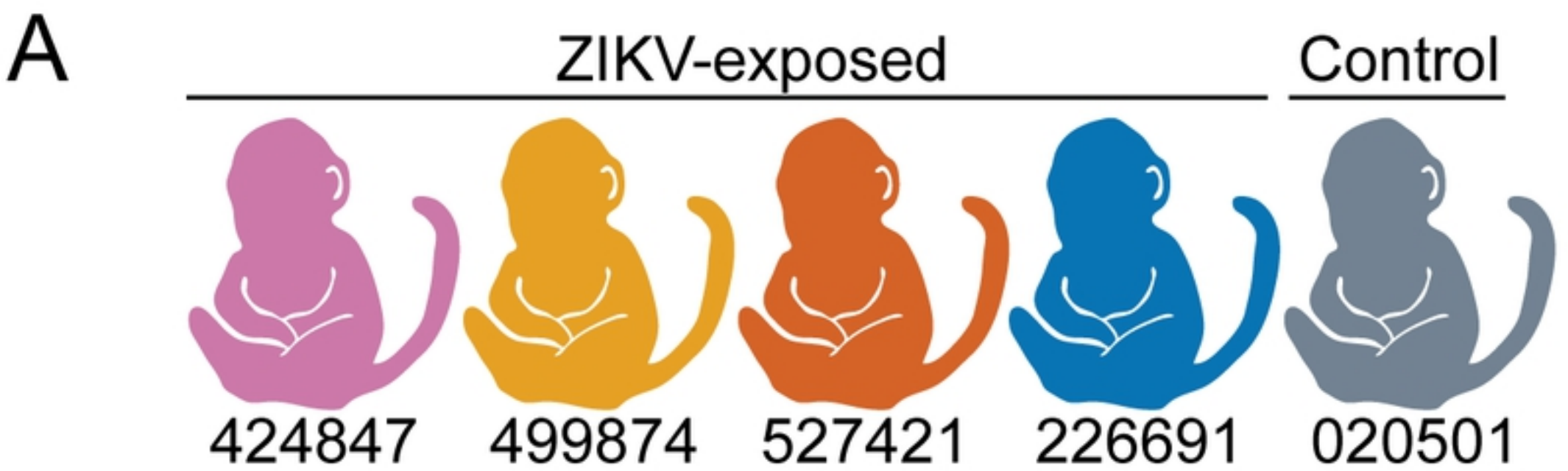

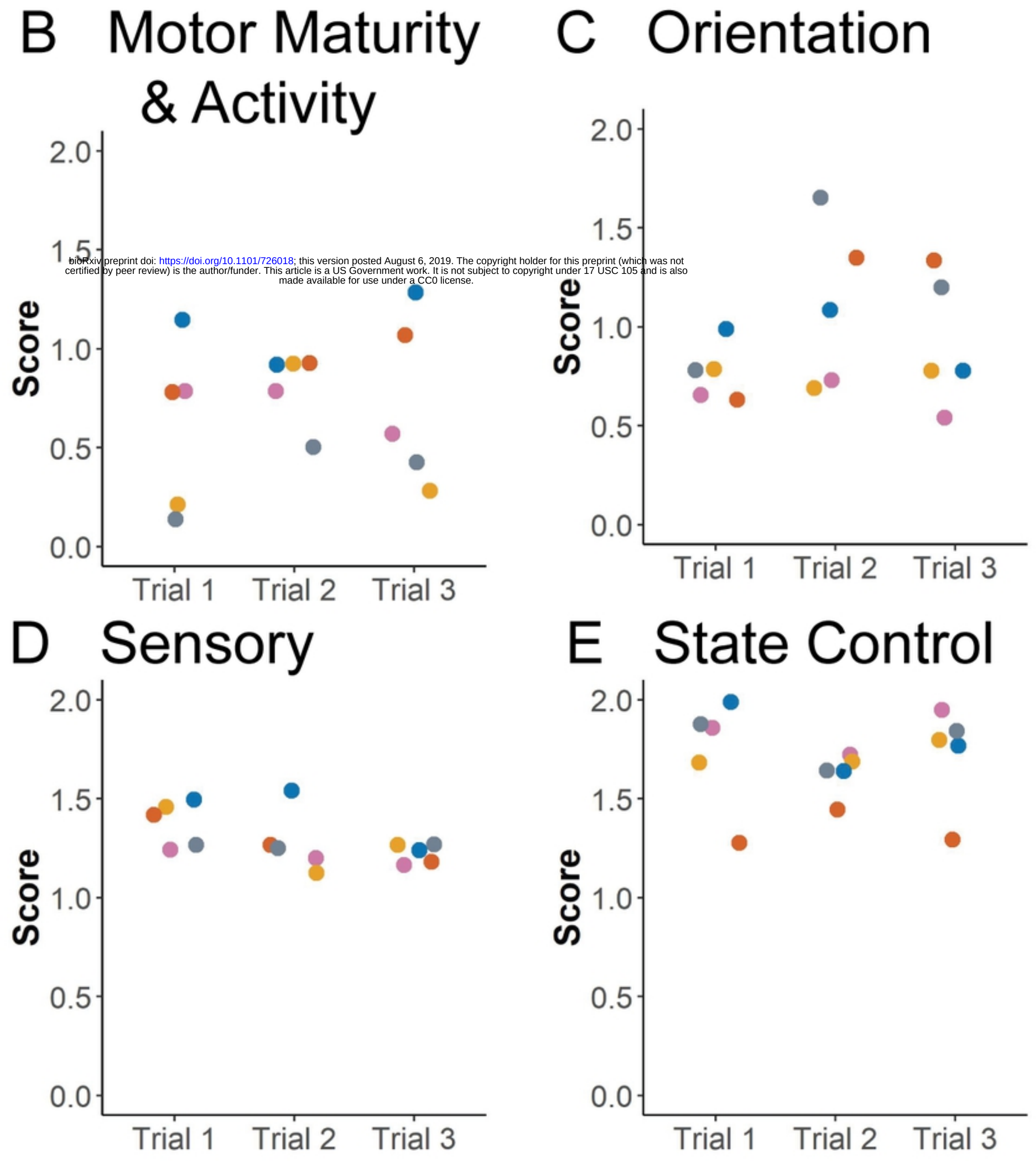

Figure 6